REVIEW OF PREFRACTURING TESTING AND EFFECT OF MEASURED PARAMETERS ON FRACTURE DESIGN

Saeed Hedayati and Hazim H. Abass
Halliburton Services

Mohamed Y. Soliman
Halliburton Reservoir Services

Doug Boyd
Halliburton Logging Services

ABSTRACT

Realistic design of a hydraulic fracture requires prior knowledge of several fluid and formation parameters. Some of these parameters are (1) mechanical properties of the rock, (2) in-situ stresses in both pay zone and adjacent zones, and (3) fluid leakoff properties. Some of the methods used in the oil field industry to measure or calculate these parameters are (1) microfrac tests, (2) anelastic strain recovery, (3) full-wave sonic log, and (4) minifrac tests.

The proposed paper briefly addresses current knowledge of hydraulic fracture design. Within this paper, the authors review each of the above methods and present the state-of-the-art techniques that were used to analyze collected data. This paper also presents the effect of each of the parameters on the design of hydraulic fracturing with several field examples given to show the practical aspects of these methods.

In summary, this paper:

1. Condenses the voluminous literature and theories on microfrac tests, anelastic strain recovery, full-wave sonic log, and minifrac tests.

2. Provides convenient reference for the literature on prefrac tests.

3. Gives insight into different methods of analyzing prefrac tests and their effects on hydraulic fracturing design.

4. Shows the feasibility of these methods through field examples.

INTRODUCTION

Hydraulic fracturing was introduced to the oil industry in 1947 with the stimulation of a gas well in the Hugoton gas field in Grant County, Kansas. Over the years since 1947, the size of fracture stimulation treatments has grown from a few hundred gallons to more than a million gallons of fluid with placement of several million pounds of sand. Meanwhile, many technologies and theories were developed in the 1970's and 1980's, enabling engineers to design and optimize a hydraulic fracturing job to increase early production and increase the rate of return on investment.

The hydraulic fracturing process consists of injecting a sequence of prepad, pad, and proppant-laden fracturing fluid into the wellbore at a rate far exceeding that permitted by rock matrix. When the applied pressure exceeds the fracture pressure, the rock will fracture and proppant is placed into the induced fracture to hold it open. Fractures usually propagate in planes perpendicular to the direction of the least principal stress. Well productivity is enhanced by exposing a large area of the reservoir to essentially wellbore pressure.

Any process can be divided into three major components: (1) input, (2) system and (3) output. The hydraulic fracturing process also can be categorized in the following manner, which is depicted in Fig. 1.

1. Input: Main components are fracturing fluid, proppant, chemicals, and equipment.
2. System: Consisting of wellbore and reservoir.
3. Output: A hydraulic fracture connecting the wellbore to a large portion of the reservoir.

The ultimate output of the hydraulic fracturing process is production increase; hence, increase in revenue. Figure 2 depicts the concept of optimization considering production increase and cost as a function of treatment volume.[1] Success of the process and optimum output (production increase) are contingent on data and information gathered from the system (reservoir), which in turn affect the components of input to the process. There are interactions between input, system, and output that should be considered in the design of hydraulic fracturing. For example, fracturing fluid (input) can damage reservoir permeability (system) and fracture conductivity (output). Many fracturing processes are designed and optimized for the output (production increase). Production increase is a function of fracture length, fracture conductivity, and original reservoir properties such as permeability and porosity. The system (reservoir) properties can be divided into two parts:

1. Reservoir Properties: This includes porosity, saturation, permeability, reservoir pressure, etc.

2. Mechanical Properties: This includes Poisson's Ratio, Young's modulus, critical stress intensity factor, in-situ stress, etc.

In this paper, we have studied three of the most common methods that are used in measurement of the magnitude and direction of in-situ stresses. These methods are microfrac, anelastic strain recovery, and full-wave sonic log. The in-situ stresses play an important role in well location pattern in a given field, proppant design, and fracture height growth.

Well Location Pattern

The induced hydraulic fracture is normally perpendicular to the minimum in-situ stress. Lemon *et al.*[2] and Holditch[3] studied the effect of drainage area and shape on the placement of a vertically fractured well. Their simulation work showed that production increase is dependent on drainage, permeability, fracture length, and fracture conductivity. To optimize the number of wells drilled to drain a given field, the wells should be closely spaced in the direction of minimum horizontal stress. This is because the induced fractures will be perpendicular to the direction of minimum horizontal stress, and therefore the drainage shape will be irregular.

Proppant Selection

Proppants help prevent the fracture from closing once injection is stopped and provide a highly permeable conduit for hydrocarbon to flow toward the wellbore. Crushing and embedment may cause proppant to fail in providing high conductivity. Proppant particles must have enough strength to support the closure stress and prevent crushing.[4] The magnitude of the closure stress depends on the least in-situ principal stress, the reservoir pressure, and the flowing bottomhole pressure at the time of production. Proppant bed concentration and rock strength control the effect of embedment on proppant conductivity. If embedment is expected, proppant bed concentration (i.e., propped fracture width) should be increased to compensate for the loss in productivity.

Fracture Height Growth

Minimum horizontal in-situ stress distribution and treatment pressure are the main controlling factors of fracture height. The stress-intensity factor equations used to predict the fracture height were given by Rice.[5] Rice's equation involved few integrals. Using several assumptions, Simonson[6] solved these integrals, giving equations relating fracturing height, rock properties, in-situ stress distribution, and wellbore injection pressure. Ahmed *et al.*[7] enhanced the Simonson *et al.* solution by including gravity effects and used it for wells with multiple layers. The fracture height growth is given by the following two equations.

$$\Delta p = p_{wt} - p_{ext} = C_1 \left[K_{IC} \left(\frac{1}{\sqrt{h_u}} - \frac{1}{\sqrt{h}} \right) + C_2 \left(\sigma_b - \sigma_a \right) \cos^{-1} \left(\frac{h}{h_u} \right) \right] + C_3 \rho g \left(h_u - \frac{h}{2} \right) \tag{1}$$

$$\Delta p = p_{wt} - p_{ext} = C_1 \left[K_{IC} \left(\frac{1}{\sqrt{h_d}} - \frac{1}{\sqrt{h}} \right) + C_2 \left(\sigma_c - \sigma_a \right) \cos^{-1} \left(\frac{h}{h_d} \right) \right] + C_3 \rho g \left(h_d - \frac{h}{2} \right) \tag{2}$$

and $h_t = h_u + h_d - h$

h, h_t, h_u, h_d	=	see Fig. 3
Δp	=	net pressure; pressure above the initial fracture extension pressure
p_{wt}	=	wellbore treatment pressure
p_{ext}	=	fracture extension pressure
σ_b	=	upper barrier minimum in-situ horizontal stress
σ_a	=	pay zone minimum in-situ horizontal stress
σ_c	=	lower barrier minimum in-situ horizontal stress
K_{IC}	=	critical stress intensity factor
ρ	=	density of fracturing fluid
C_1,C_2,C_3	=	numerical constants

The relationship between h_t, h_u, and h_d is depicted in Fig. 3. By neglecting gravity effect and substituting numerical values for C_1 and C_2, Eqs. 1 and 2 can be written as:

$$\Delta p = p_{wt} - p_{ext} = \frac{1}{\sqrt{\pi}} K_{IC} \left(\frac{1}{\sqrt{h_u}} - \frac{1}{\sqrt{h}} \right) + \frac{2}{\pi} \left(\sigma_b - \sigma_a \right) \cos^{-1} \left(\frac{h}{h_u} \right) \tag{3}$$

$$\Delta p = p_{wt} - p_{ext} = \frac{1}{\sqrt{\pi}} K_{IC} \left(\frac{1}{\sqrt{h_u}} - \frac{1}{\sqrt{h}} \right) + \frac{2}{\pi} \left(\sigma_c - \sigma_a \right) \cos^{-1} \left(\frac{h}{h_u} \right) \tag{4}$$

Later in this paper we will cover minifrac applications. This process consists of a series of tests performed over a fracture interval to determine formation response to fracturing. Minifrac testing consists of three procedures, namely step rate, pump-in/flowback, and pump-in/shut-in. Most people in the oil industry consider only the pump-in-shut-in as a minifrac. Many in the industry group the minifrac and microfrac tests together, which leads to confusion. Therefore, they will be addressed separately here.

MICROFRAC TESTING

The name "microfrac" infers a small hydraulic fracture. Many authors such as Hurbert and Willis,[8] Fairhurst,[9] Kehle,[10] and others have shown that a small frac job can be used to measure the minimum in-situ stress ($\sigma_{H,min}$), magnitude, and direction. In the procedure, a small volume of fluid is injected at a low and constant flow rate which exceeds what the matrix permeability can accommodate. The bottomhole pressure is increased until a fracture is initiated at the wellbore, then the fracture is allowed to extend for a few minutes, and subsequently the well is shut-in. The pressure performance is then analyzed to determine the magnitude of minimum in-situ stress. Several methods have been suggested to evaluate this parameter. The pressure behavior during a microfrac is depicted in Fig. 4. The estimate of minimum horizontal stress from a microfrac test has been the subject of debate in the last few years. Microfrac testing can be performed in both open hole and cased hole. In both cases, a magnitude of stress is measured, but in open hole, an oriented core could also be retrieved, and direction of minimum stress also ascertained.

In-Situ Stress

Every point in the reservoir is subjected to many stresses from many directions. It can be proved mathematically that any system of stresses acting at any point can always be resolved by three orthogonal stresses, which are called the principal stresses. These three stresses exerted at a point are typically labeled the maximum, intermediate, and minimum principal stresses. In many reservoirs, the maximum stress is essentially vertical (σ_v), which is the overburden force. The other two stresses, therefore, will generally be in a horizontal plane and perpendicular to each other. The smaller of these two horizontal stresses is called minimum horizontal stress ($\sigma_{H,min}$) and the larger one is called maximum horizontal stress ($\sigma_{H,max}$).

The minimum horizontal stress has been referred to as:

1. In-situ stress

2. Least in-situ stress
3. Minimum in-situ stress
4. Closure pressure
5. Fracture closure pressure
6. Minimum principal stress
7. Least principal stress
8. Least principal horizontal stress
9. Least compressive stress

Before pressurization of the wellbore, the tangential (hoop) stress at the wellbore periphery is in compression. When the pressure is increased, the tangential stress becomes tensile, and this tensile stress must reach the tensile strength, σ_{to}, of the rock so that the minimum and maximum horizontal principal stresses can be calculated from a hydraulic fracturing test using the following equation:

$$\sigma_{H,\max} = \sigma_{to} + 3\,\sigma_{H,\min} - p_b - p \quad (\textit{assuming that tectonic stress is negligible}) \tag{5}$$

$$\sigma_{H,\min} = \textit{minimum in-situ stress} \qquad (\textit{from the microfrac test})$$

where:

$\sigma_{H,max}$	=	Maximum horizontal stress, psi
$\sigma_{H,min}$	=	Minimum horizontal stress, psi
p_b	=	Breakdown (fracture initiation) pressure, psi
p	=	Pore pressure, psi
σ_{to}	=	Tensile strength of rock, psi

Pore pressure is same as the reservoir pressure and is estimated from drillstem testing or other reservoir testing. The breakdown pressure is the maximum pressure observed in the beginning of fracturing process, which reflects the pressure required to initiate a fracture at the wellbore periphery. The tensile strength of the rock is measured in the lab. Field observations very often disagree with predictions using Eq. 5. This is most likely due to poor communication of the hydraulic pressure to the reservoir since very few wells are fractured with open hole completions.

Several years ago the minimum horizontal stress was estimated by equating it to the instantaneous shut-in pressure (ISIP). ISIP is the pressure measured immediately after shut-in following a fracturing treatment. The difference between the last treatment pressure before shut-in and ISIP reflects the fluid friction pressure from the tip of the fracture to the point where the pressure is being measured. For a relatively high fluid loss system, ISIP may be a fair estimate of minimum in-situ stress. Recently, several methods have been suggested to analyze the fall-off pressure and estimate the fracture closure pressure (FCP). This fracture closure pressure is then used as an estimate of the minimum horizontal stress.

Microfrac Test Procedure

The test is usually performed at very low injection rates of 3 to 25 gal/min over a short period of time. The well is shut-in and the pressure fall-off is monitored. This microfrac procedure is repeated about three times. Figure 5 shows pressure response in the microfrac tests process. Field tests are either performed in open hole or cased hole. There are some advantages and disadvantages to both methods, and they will be briefly discussed below:

Openhole Microfrac Test

In this test, the zone of interest is isolated with an impermeable plug, such as an openhole testing packer. If a microfrac were to be performed at the bottom of the well, one packer would be sufficient for isolation. Figure 6 shows an overall picture of the open hole microfrac process. A surface readout, a downhole pressure-temperature gauge, or a memory gauge may be used to gather bottomhole pressure data.[11] In this procedure, drilling mud is used as a pumping fluid, and an oriented core can be retrieved from the bottom of the hole to evaluate the direction of minimum in-situ stress.[12] The advantages and disadvantages of openhole microfrac testing can be summarized as follows.

Advantages:

1. The procedure can be performed during drilling.
2. Drilling mud can sometimes be used.
3. Fractured core may be retrieved.

Disadvantages:

An incompetent borehole (not round), an unconsolidated formation, a washout, or a highly naturally fractured formation cause problems.

Cased Hole Microfrac Test

This procedure is similar to openhole microfrac testing. Mechanically, it is easier to perform since the procedure is performed in a cased hole. The downhole equipment assembly is shown in Fig. 7. Either packer and bridge plug or straddle packer assemblies can be used. The advantages and disadvantages of this test are as follows.

Advantages:

1. Mechanically simpler; packer and bridge plug combination or straddled casing packers may be used to isolate 4 to 20 ft of zone of interest.
2. A competent borehole is not required.
3. It can test several zones in one day.

Disadvantages:

1. Fractured core is not retrieved, hence, no knowledge of direction of minimum in-situ stress is gained.
2. Perforation and cement may affect the procedure and analysis of the data.

Microfrac Analysis

As mentioned earlier, the main purpose of microfrac testing is to determine the fracture closure pressure, which is an estimate of least principal stress. After termination of pumping, the shut-in pressure is analyzed. In extremely low-permeable formations, it may take a long time for the pressure to experience appreciable decline; therefore, a modified procedure called "pump-in/flowback" is used to obtain the required data. The microfrac flowback example is shown in Fig. 8. It shows how the fracture closure pressure (FCP) is picked from the pressure profile. From the shut-in or fall-off pressure, two pressures are determined, instantaneous shut-in pressure (ISIP) and fracture closure pressure (FCP).

ISIP

This is the pressure measured immediately after shut-in, which is approximately equal to the final bottomhole treating pressure (BHTP) minus friction pressure. In appropriate reservoirs, ISIP is a fair estimate of minimum shut-in stress.

FCP

This pressure[13] is defined as:

1. Pressure required to hold the fracture open after initiation.

2. Pressure required to hold the fracture from just closing.

FCP is considered a good estimate of minimum in-situ stress.

Methods of Analysis

There are two methods of estimating a value for minimum in-situ stress, the ISIP method and the flow regime change method.

ISIP Methods

There are several techniques available to determine the minimum in-situ stress from shut-in curves:

1. Inflection Point Technique: This method explained by Gronseth and Kry[14] consists of drawing a line tangent to the shut-in pressure curve immediately at the shut-in point. The shut-in pressure is the pressure at the point at which the shut-in pressure curve diverges from the tangent line.

2. McLennan Methods: In his PhD thesis, McLennan[15] proposed three methods: (1) the pressure value at the intersection of two tangent lines drawn to initial and end parts of the shut-in curve, (2) the pressure value at the point of maximum curvature, and (3) the pressure value where the shut-in curve levels off.

3. Log (pressure) vs. log (time) technique: This method described by Zoback and Haimson,[16] selects a shut-in pressure as the pressure point where the slope of the curve

changes. The curve under consideration is the log (shut-in pressure) vs. log (time).

4. Pressure vs. log (time) technique: This technique recommended by Doe[17] is similar to the method described in 3. The only difference is the curve under consideration is the shut-in pressure vs. log (time).

5. Pressure vs. $\log\left(\frac{t + \Delta t}{\Delta t}\right)$: This method, which is reminiscent of a Horner plot, is recommended by McLennan and Roegiers.[18] In this technique t is the pumping time, and Δt is the time since shut-in. The shut-in pressure is the pressure at the inflection point of the curve.

6. Ln(pressure) vs. time technique: This technique, introduced by Aamodt and Kuriyagawa,[19] is more involved. The shut-in pressure is determined by: (1) plotting $\ln(p-p_a)$ vs. time; (2) assuming p_a which is the asymptotic value of shut-in pressure and p which is the shut-in pressure; (3) picking several p_a values and continuing to plot them until the best straight line fit is found; (4) the fitted straight line to the shut-in time of zero, resulting in pressure value of p_e; and (5) assuming the shut-in pressure is the sum of p_a and p_e.

Aggson and Kim[20] reported the results of in-situ stress analysis from an extensive series of hydraulic fracturing tests done at Hanford site in southeastern Washington state for the purpose of investigating the feasibility of disposing of nuclear wastes. They reported that method 6 consistently gave the highest shut-in pressure, with methods 3 and 4 giving low shut-in pressures. Methods 1 and 5 usually gave a median value.

Flow Regime Change Analysis

Fluid flow equations for a reservoir with finitely conductive fracture were developed by Cinco-Ley[21] in the late 1970's. He postulated that for a finitely conductive fracture reservoir, both linear and bilinear flow regimes may exist. The linear flow pressure response has a half slope on a log-log graph of $\Delta p = p_i - p_{wf}$ vs. time (where p_i and p_{wf} are static reservoir pressure and wellbore flowing pressure, respectively) and the plot of Δp vs. square root of time is a straight line. Similarly the bilinear flow response has a slope of one-fourth, and a plot of Δp vs. fourth square root of time is a straight line. Nolte[22] used the above observations in analyzing the fracture shut-in pressure and eventual evaluation of closure pressure. The purpose of flow regime change technique is to detect the end of fracture flow during the pressure decline and can be briefly summarized as follows:

1. The log-log plot of Δp vs. time exhibits a half slope. The end of half slope is the end of fracture flow, and fracture closure pressure is evaluated at that point. In this case, Δp represents the difference between the instantaneous shut-in pressure, p_{isip}, and shut-in pressure, p_s. Some people define Δp as the difference between the final injection pressure, p_{fi}, and shut-in pressure, p_s. Figure 9 shows a log-log plot of pressure fall-off. Fracture closure pressure is determined from the end of half slope.

2. The plot of Δp vs. $\sqrt{time}$ exhibits a linear behavior. When the line starts to curve, the fracture starts to close, and the fracture closure pressure can be evaluated from that point. The term Δp here is the same as defined above. Figure 10 shows a square root of time analysis. Fracture closure pressure is found from the end of linear part of fall-off curve.

Jones and Sargeant[23] introduced bilinear flow and pressure derivative analysis in obtaining the minimum horizontal stress from microfrac data.

Field Example

The microfrac procedure has been used in reservoirs in the development stages to estimate the magnitude and direction of in-situ stress.[12,24-26] A microfrac test was performed on a well at a depth of 2620 ft with 9.20 lb/gal drilling mud. The test was performed in three different injection/shut-in stages as shown in Fig. 11. The first stage was performed at an average rate of 65 gal/min as shown in Fig. 12. Pressure vs. square root of time analysis gives the end of linear flow at 260 psi. This pressure corrected to the bottomhole conditions give a fracture closure pressure of 1500 psi. Figure 13 shows a tubing pressure vs. $\sqrt{time}$ plot for the first stage. The second stage was performed at an average rate of 6.0 gal/min. Closure pressure for this stage was determined to be 1460 psi. Injection 3 was performed at 6.5 gal/min. After shut-in, the packer slipped resulting in bad shut-in data, and omission of last stage data. This example shows the importance of several injection/shut-in stages in microfrac testing.

ANELASTIC STRAIN RECOVERY

The determination of the in-situ state of stress in petroleum reservoirs from anelastic strain recovery (strain relaxation) of an oriented core is an extension of the in-situ stress determination method called "borehole deformation," which is also referred to as "overcoring." Magnitude of stresses is an important factor to consider in the mining industry to make provisions to keep mine shafts stable and safe. Direction of stresses has also been measured in mine fields; however, it is not as important as the difference in magnitude of stresses for some applications.

In the oil industry, as was emphasized earlier, direction and magnitude of stresses are crucial to the design of an optimum hydraulic fracturing treatment. Six methods have been proposed in the mining industry to measure the absolute stress of rock: (1) borehole deformation, (2) flatjack, (3) seismic wave velocity, (4) hydraulic fracturing, (5) core discing, and (6) static equilibrium method.[27] The propagation velocity method uses the propagation wave velocities of sound in rock to find modulus of elasticity, E, and a Poisson's Ratio, ν, in terms of magnitude of stresses. This method has been extended to the oil industry with the development of the full-wave song log, which will be discussed in detail later. Hydraulic fracturing was suggested as a good method to gain some knowledge about the stress state in underground mining.[9-10] The hydraulic fracturing method has been used extensively in the oil industry to measure the magnitude and direction of stress of reservoir rock, and a test named "microfrac tests" was developed, which was discussed earlier.

Elastic and Anelastic Deformation

When a core is removed from the reservoir rock, it undergoes elastic and anelastic expansion.

The elastic component is instantaneous, while the anelastic displacement is a function of time and the expansion of core may take 5 to 60 hours to be complete. Figure 14 shows the displacement vs. time curve for a core removed from a reservoir. This figure shows the instantaneous elastic component ($\Delta\varepsilon_e$) and anelastic component ($\Delta\varepsilon_t$). In the petroleum industry only the anelastic component is used to evaluate the direction of in-situ stresses. Some anelastic displacement (BC') is lost while the remaining oriented core is being retrieved from the oil reservoir. The anelastic diametrical displacement component (C'C) is measured with accurate instruments, and information is used to calculate the direction of in-situ stresses.

Anelastic Strain Recovery

Anelastic strain recovery (ASR) or strain relaxation (SR) was first introduced to the oil industry in the early 1980's.[28-29] Strain recovery in the anelastic process is the result of microcrack formation and expansion. Since microcracks are formed uniformly throughout the core, the expansion is in all directions. This fact has been substantiated from the fact that a direct correlation exists between differences in velocity and elastic modulus relative to the strain recovery and elastic modulus relative to the strain relaxation magnitudes from the oriented core.[28] The magnitude of recovered strain in any direction is proportional to the magnitude of the in-situ stress in the same direction. Therefore, the minimum and maximum recovered displacements (strains) are in the minimum and maximum in-situ stress directions, respectively. Figure 15 shows how a cylindrical core retrieved from the reservoir relaxes and changes dimensions.

Assumptions

The following idealized assumptions are made to extend the elastic theories and evaluate the direction of in-situ stresses.[30]

1. Core must be homogeneous and linearly viscoelastic.

2. The creep must be isotropic.

3. Poisson's Ratio of the rock must remain the same with the elapse of time.

4. The core must be free of cracks or natural fractures.

5. The core should have isotropic thermal properties.

Components of Core Deformation

The expansion of a retrieved core is the function of in-situ stress magnitudes and the following factors:

1. Change in core temperature
2. Change in pore pressure
3. Release of overburden pressure

This expansion may be negative, which is tantamount to contraction. The following formula gives the net diameter displacement of the core.

$$\Delta D = \Delta D_{st} - (\Delta D_p + \Delta D_{ov} + \Delta D_t) \tag{6}$$

Where ΔD_p is the diametrical displacement caused by the pore pressure. The release of pore pressure and loss of moisture causes contraction of core. Some operators try to minimize this contraction by sealing the retrieved core sample. The ΔD_t term is the thermal component. It contributes as a contraction since the core is moved from the hot environment to the cold area. The term ΔD_{ov} is the diametrical contraction of the core when the overburden stress is removed. Term ΔD_{st} is the diametrical expansion of the core sample due to the release of unequal in-situ horizontal stresses. Terms ΔD_p, ΔD_{ov}, and ΔD_t components act rapidly and uniformly in all directions; however, the ΔD_{st} component of radial displacement is directional. It is maximum in the direction of maximum in-situ stress and minimum in the direction of minimum principal stress. Therefore, measured displacement (ΔD) reflects the directional diametrical changes caused by in-situ horizontal stresses.[30]

Theory

In practice, the directions of principal strains usually are not known; however, if strain is measured in three arbitrary directions (α, β, γ), then the magnitude and direction of the principal strains may be calculated. A strain rosette is used to measure a unit elongation at a point in three directions. The equations used to determine the state of strain depend on the arrangement of the strain rosettes. The formulas for the equiangular arrangement to calculate the displacement (strain) in the maximum and minimum in-situ directions and the orientation of the principle strains will be discussed. In this arrangement, diametrical displacements are measured 60° apart on the circumference of the core. The direction of the principal strains is calculated using the following equation:

$$\theta = \frac{1}{2} \tan^{-1} \frac{\sqrt{3}(\epsilon_\beta - \epsilon_\gamma)}{2\epsilon_\alpha - (\epsilon_\beta + \epsilon_\gamma)} \tag{7}$$

Where θ is the acute angle from the α axis to the direction of the nearest principal strain. ε_α, ε_β, and ε_γ are the strains measured in the α, β, and γ directions. These axes are 60° apart. The magnitude of minimum and maximum principle strains are given by the following two equations:

$$\epsilon_I = \frac{1}{3} \left[\epsilon_\alpha + \epsilon_\beta + \epsilon_\gamma + \sqrt{2 \left[(\epsilon_\alpha - \epsilon_\beta)^2 + (\epsilon_\beta - \epsilon_\gamma)^2 + (\epsilon_\gamma - \epsilon_\alpha)^2 \right]} \right] \tag{8}$$

$$\epsilon_{II} = \frac{1}{3} \left[\epsilon_\alpha + \epsilon_\beta + \epsilon_\gamma - \sqrt{2 \left[(\epsilon_\alpha - \epsilon_\beta)^2 + (\epsilon_\beta - \epsilon_\gamma)^2 + (\epsilon_\gamma - \epsilon_\alpha)^2 \right]} \right] \tag{9}$$

The minimum and maximum horizontal strains will be inferred from E_I and E_{II}. As we can see, from the formulas we can only infer the direction of in-situ stresses. Ratio of maximum to minimum principal stresses is given by dividing Eqs. 8 and 9. However, several attempts have been made to estimate the magnitudes of principal stresses.

Estimation of Principal Stresses

The viscoelastic theory for rock mechanics is used to estimate the magnitude of principal stresses. Two cases of anelastic recovery of isotropic and transversely isotropic media were considered.[31] The following assumptions were made to derive the formulas.

1. The rock is homogeneous and linearly viscoelastic.
2. In-situ stresses are removed instantaneously.
3. Poisson's Ratio is not time dependent.

Blanton[31] gave these estimates for the isotropic and transversely isotropic media:

1. In an isotropic case, only Poisson's Ratio of the material is required. The estimates of principal stresses for this case are given by the following two equations:

$$\sigma_x = \sigma_z \frac{(1-\nu)\,\Delta\epsilon_x + \nu\,(\Delta\epsilon_y + \Delta\epsilon_z)}{(1-\nu)\,\Delta\epsilon_z + \nu\,(\Delta\epsilon_x + \Delta\epsilon_y)} \tag{10}$$

$$\sigma_y = \sigma_z \frac{(1-\nu)\,\Delta\epsilon_y + \nu\,(\Delta\epsilon_x + \Delta\epsilon_z)}{(1-\nu)\,\Delta\epsilon_z + \nu\,(\Delta\epsilon_x + \Delta\epsilon_y)} \tag{11}$$

$\sigma_x, \sigma_y, \sigma_z$ = In-situ principal stress magnitudes
$\Delta\varepsilon_x, \Delta\varepsilon_y, \Delta\varepsilon_z$ = Differential principal strain recoveries
υ = Isotropic Poisson's Ratio

2. For the transversely isotropic case, two Poisson's Ratio terms, as well as the ratio of strain recoveries, are required. These two estimates are given by the following two equations:

$$\sigma_x = a\,\sigma_z \frac{(1-\nu_2^2 a)\,\Delta\epsilon_x + (\nu_1 + \nu_2^2 a)\,\Delta\epsilon_y + (1+\nu_1)\,\nu_2\,\Delta\epsilon_z}{(1+\nu_1)\left[(1-\nu_1)\,\Delta\epsilon_z + \nu_2 a\,(\Delta\epsilon_x + \Delta\epsilon_y)\right]} \tag{12}$$

$$\sigma_y = a\,\sigma_z \frac{(1-\nu_2^2 a)\,\Delta\epsilon_y + (\nu_1 + \nu_2^2 a)\,\Delta\epsilon_x + (1+\nu_1)\,\nu_2\,\Delta\epsilon_z}{(1+\nu_1)\left[(1-\nu_1)\,\Delta\epsilon_z + \nu_2 a\,(\Delta\epsilon_x + \Delta\epsilon_y)\right]} \tag{13}$$

a = Ratio of strain recoveries
$\sigma_x, \sigma_y, \sigma_z, \Delta\varepsilon_x, \Delta\varepsilon_y$, and $\Delta\varepsilon_z$ are the same as in the isotropic case
υ_1, υ_2 = Transversely isotropic Poisson's Ratio

Instrumentation and Equipment

Anelastic strain recovery is usually performed with openhole microfrac tests. To determine fracture orientation (azimuth) in openhole microfrac tests, an oriented core is retrieved from the reservoir.

From this core, several small cylindrical core samples are procured to be used in anelastic strain recovery equipment. Anelastic strain data missed during tripping out of the hole are believed to account for the greater percentage of the total strain to be recovered. Therefore, a reliable, stable, and sensitive monitoring device is required to measure the remaining strain, which is only a few hundred microns. The monitoring device is usually interfaced with fast computers, where the data are stored, and is analyzed with available programs. Test apparatuses have been developed so that vertical well cores and cores retrieved from deviated wells can be tested. These apparatuses are similar with few changes described below.

Vertical Hole Sample Apparatus

This apparatus consists of six digital displacement transducers evenly spaced around the circumference of the core sample. These transducers are arranged such that the lateral creep in the core is measured at 120° intervals. The vertical growth of the core is measured by an additional transducer. The seven displacement measurements that are read from these transducers are recorded with the data acquisition system. Figure 16 shows a vertical hole sample data gathering system.

Deviated Hole Sample Apparatus

The device used to test oriented cores retrieved from deviated wells is similar to vertical hole core apparatus; however, more displacements are measured as described below:

1. Eighteen transducers in three layers of six transducers are placed around the circumference of the core sample similar to the vertical well testing device.

2. Four transducers measure the vertical displacements of the sample to define the tilt of the upper core surface.

This type of apparatus has been used to measure the direction of fracture in deviated wells as reported by El Rabaa.[32] The apparatus for recovering anelastic strain from deviated wells is shown in Fig. 17.

Field Example

Anelastic strain recovery has been used successfully to estimate the direction of minimum principal stress in the lab and in the field.[30,32-33] Here we give an anelastic strain recovery analysis. This analysis was performed on data collected from an oriented core sample that was retrieved from the reservoir after microfrac test. The displacement data is shown in Fig. 18; x, y, and z displacements are measured 60° apart around the core sample. Incorporating the measured displacements in appropriate equations gives the azimuth of the maximum strain. Figure 19 gives the plot of elapsed time vs. azimuth of maximum strain. The azimuth results are calculated using moving increments. The calculated azimuth for each increment is based upon the displacement change between a starting point and an end point separated by 20 data values. Statistical analysis of results in Fig. 19 are given in Fig. 20. Note that in the figures the direction of maximum stress or the direction of induced fracture is given. Also, the major scribe line (MSL) on the retrieving core is 68.6 clockwise (CW) of north and 10° clockwise (CW) of x-axis. The x-axis corresponds to the position on the core where the x-displacement is measured. From Fig. 20 we can see that the azimuth of induced fracture is about 83°.

DETERMINATION OF IN-SITU STRESS FROM FULL-WAVE SONIC DATA

Measurement of shear wave/compressional wave slowness presently is the most economical method of predicting minimum horizontal stress. Faith in the stress predictions requires calibration to actual stress data from a program of microfracs. Microfrac calibration data must be taken not only in the reservoir rock but in the bounding lithologies. The correlations derived usually are applicable only to those particular formations over a limited geological area.

Basic Theory

Elastic theory states vertical stress induces horizontal stress, if the horizontal layers are laterally confined. Vertical stress magnitude can be transformed to horizontal stress using a coupling factor ($\nu / (1 - \nu)$). Poisson's Ratio, ν, is a static measurement performed on a core under simulated reservoir conditions.

$$\sigma_H = \frac{\nu\ (static)}{1 - \nu\ (static)} * \sigma_v \tag{14}$$

where:

σ_H = Horizontal stress
σ_V = Vertical stress (for geologic formations, overburden weight)
ν = Static Poisson's Ratio

For geological formations, a good approximation of vertical stress is obtained through integration of the bulk density log from formation depth to surface. Typical values of overburden stress are 1.01 to 1.1 psi/ft.

Dynamic Vs. Static Poisson's Ratio

Full-wave sonic tools measure compressive and shear wave slowness. The travel times of these sound waves are affected by the longitudinal and lateral deformation characteristics of the rock. The dynamic Poisson's Ratio may be obtained as follows:

$$Poisson's\ Ratio\ (dynamic) = \frac{2 - DTS^2 / DTC^2}{2\,(1 - DTS^2 / DTC^2)} \tag{15}$$

DTS = Travel time of shear wave
DTC = Travel time of compressive wave

Use of Eq. 14 requires static Poisson's Ratio. This may be obtained through a calibration of static vs. dynamic Poisson's Ratio. Conflicting investigations have determined dynamic Poisson's Ratio to be less or greater than static Poisson's Ratio.[34-37] Static to dynamic ratios vary substantially depending on whether the measurement was performed on dry or fluid saturated samples. In saturated rocks, Poisson's Ratios exceed that of dry samples.[37-39] Increasing effective stress (the difference between confining pressure and pore pressure) decreases "wet" Poisson's Ratio.[38] Possible reasons for the poor match between dynamic and static Poisson's Ratio include: (1) moisture sensitivity, (2) rock crack closing, (3) experimental technique, (4) temperature, (5) sample anisotropy, (6) hysteresis, and (7) rate of stress application.

To calibrate dynamic Poisson's Ratio to the static Poisson's Ratio, core must be available. The core plugs should be orientated vertically and in-situ confining pressure and pore pressure duplicated to obtain accurate static measurements. Core plugs are small in comparison to the rock mass that the acoustic tool investigates. Dynamic lab measurements of each sample are useful in surmounting this. Should no static rock property information be available, no adjustment to dynamic Poisson's Ratio may be performed. One such calibration is presented in Fig. 21.

Pore Pressure

Pore pressure (p) works against confining stress (S). Terzaghi[40] expressed effective stress as the difference between total stress and pore pressure.

$$\sigma = S - P \qquad (16)$$

where:

P	=	Pore pressure
σ	=	Effective stress
S	=	Total stress

Handin *et al.*[41] modified the equation by applying a correction factor (α) to the pore pressure term.

$$\sigma = S - \alpha P \qquad (17)$$

The factor, α, accounts for the deformation of the rock framework and the subsequent inefficiency in the transmission of pore pressure. The effect of pore pressure in counteracting the confining pressure is therefore reduced. Typical values for α are 0.65 for limestone, 0.6 for sandstone, and 0.7 for dolomite.[37] The factor, α, may be evaluated as follows:

$$\alpha = 1 - \frac{C_r}{C_b} \qquad (18)$$

where C_r	=	Matrix compressibility, psi^{-1}
and C_b	=	Bulk compressibility, psi^{-1}

This equation assumes the ideal case, i.e., there is no porosity change under equal variation of pore pressure and confining pressure.[42]

The concept of effective stress has caused some confusion when it is applied to field problems; therefore, it deserves some explanation and elaboration. The following hypotheses are considered to clarify the concept of effective stress:

1. If we apply a total stress, s, on a piece of rock that is not porous (i.e., $\phi = 0$), the rock will see an effective stress equivalent to s. This is the same as if we had used Eq. 16

with pore pressure, P, equal to zero; the effective stress, σ, will be equal to S, i.e., σ = s. Equation 17 may be used to reach the same conclusion for the given hypothesis. If the rock has no porosity, the rock matrix compressibility, C_r, is equal to the bulk compressibility, C_b, causing the term α to be zero. If a zero value for α is substituted in Eq. 17, the effective stress will be equal to the applied stress, or in other words, the rock will see all the applied stress ($\sigma = s$).

2. If a total stress, s, is applied on a soil sample which has pore pressure, P, it is expected that the pore pressure will counteract the applied stress. If the applied stress is increased, the pore pressure will build up assuming that the fluid is not allowed to escape the sample (undrained). Therefore, the net effective stress applied on the soil grains is the total stress minus the pore pressure as it is proposed by Eq. 16. The same conclusion may be obtained using Eq. 17. The matrix compressibility is small compared to the bulk compressibility of the sample which causes the factor, α, to approach unity, and again the effective stress will be equal to total stress minus pore pressure.

Gas Correction

The change of a dynamic Poisson's Ratio with only a small formation gas component necessitates a gas correction to be applied. Modelling the reduction of dynamic Poisson's Ratio at varying gas saturations, Toksoz and Cheng[43] found the effect decreases with increasing depth. This is shown in Fig. 22. Anderson,[44] using Biot's theory, showed a relationship between gas saturation, porosity, and dynamic Poisson's Ratio. This relationship is depicted in Fig. 23. The magnitude of the decrease moderates with declining porosity for gas-bearing sands. Assuming an invaded zone gas saturation of 10 to 50% and knowing porosity from other open hole logs (sonic, neutron - density) the magnitude of the reduction of Poisson's Ratio because of gas may be discerned. Dynamic Poisson's Ratio can then be increased by this amount over gas-bearing intervals.

Transversely Elastic Model

The following equation, which is known as the transversely elastic equation or another form of it, is commonly applied by logging companies to calculate minimum horizontal stress.

$$\sigma_{H,\min} = \alpha * p + \frac{\nu\ (est.\ static)}{1 - \nu\ (est.\ static)} * (S_v - \alpha * p) + T \qquad (19)$$

where:

α	=	(Alpha) is a factor that accounts for pore pressure not fully counteracting overburden pressure
$\sigma_{H,\min}$	=	Minimum horizontal stress
ν	=	Poisson's Ratio (estimated static)
p	=	Pore pressure
S_v	=	Overburden stress
T	=	Other stresses (tectonic, thermal, creep, etc.)

This calculation of minimum horizontal stress assumes:

1. Formation is totally poroelastic.
2. Formation is isotropic.
3. Overburden weight is the maximum principal stress.
4. Formation is subject to lateral confinement.
5. No regional stresses.
6. No thermal stresses.
7. Static Poisson's Ratio measured from core can be used to calibrate dynamic Poisson's Ratio.

Prats[45] pointed out that Eq. 19 was inadequate in accurately predicting minimum horizontal stress. The parameter T which represents stresses due to tectonic, temperature, creep, and stress history has a significant influence on the present stress state of the formations. Rock can be highly plastic (salt, anhydrite, some shales) and frequently is not isotropic (shale). These factors call for extreme care in the application of the model. The cumulative effect of these unknowns can only be discerned through comparisons with microfrac data. Corrections to the model can then be made. Further application of the model to the same specific formations and geological area may then be carried out with confidence.

Calibration of the Transversely Elastic Equation using Minifrac/Microfrac Data

Ahmed *et al.*[46] obtained good results recognizing the limitations of modelling stresses with Poisson's Ratio. This is possible despite the frequent lack of core derived static rock properties. The key is the availability of minifrac/microfrac-derived minimum horizontal stress data. This provides calibration points which are used to correct the transversely elastic equation for stresses (T) not accounted for in the model. The procedure involves plotting the coupling factor $\nu/(1-\nu)$ (dynamic or estimated static) and pore pressure against minimum horizontal stress. This calibration method is used on four wells from four different formations in Alberta, Canada, in which a series of minifracs are performed. Figure 24 shows the location of these four wells, designated as A, B, C, and D. Also considered in this analysis is the microfrac data for a Cardium sand and shale 250 km NNW of the other four wells.[47] Fracture closure pressure, and pore pressure vs. dynamic coupling factor $\left(\frac{\nu}{1-\nu}\right)$ for these five wells is plotted in Fig. 25. A straight line connects pore pressure and fracture closure pressure. In normalizing the data to a constant pore pressure, we see that for sandstones one equation fits the data as shown by Fig. 26. However, a separate line fits the shale data. The equation that gives fracture closure pressure as a function of pore pressure and Poisson's Ratio for sandstones is given by:

$$FCP = 76.92\left(\frac{\nu}{1-\nu}\right) + p \qquad (20)$$

The above stress equation is a good predictor of minimum horizontal stress for various Alberta sandstone. This fact is ascertained by Fig. 27.

Tools and Equipment

Logging companies provide a variety of borehole acoustic tools capable of gathering shear and compressive waveforms. Monopole transmitters, multiple receivers, and transmitter-to-first-receiver spacings of 8 to 12 ft are common tool characteristics. Figure 28 is a typical tool. Dipole transmitters have recently become commercial, allowing the gathering of shear wave data in low velocity formations. Monopole transmitters fail to generate shear waves in the formation when borehole mud velocities are equal to or greater than formation velocities.

Often one logging pass over the formations of interest is all that is necessary to gather the acoustic data. Computer processing must be applied to extract the compressional and shear wave travel times from the acoustic waveforms.

Example

McLellan[47] published a study of relative in-situ stress for a Cardium sand at Wapiti, Alberta. Data gathered included dynamic/static Poisson's Ratio, overburden stress, reservoir pressure, and microfrac determined in-situ stress. He concluded that "regardless of whether laboratory or sonic log-derived dynamic elastic properties are used, simple predictions of the minimum horizontal in-situ stress may be grossly in error in this part of Alberta unless residual and active tectonic stresses are taken into account."[47] Applying his data to Eq. 19, with the proposed correction for other stresses, considerably improved sonic derived stress predictions are obtained. Accuracy is within ±8% in the Cardium sand and surrounding shales/siltstones. Figure 29 gives a caliper, gamma ray, and FCP log for the Wapiti well. From the figure we can see that the stress predictions compare favorably with the microfrac data. We can also see that little or no minimum horizontal stress contrast exists between the reservoir rock and the boundary shales. A hydraulic fracture here would have no restriction to fracture height growth and needs to be designed carefully. This points out the fallacy in assuming that shales represent stress barriers to fracture height extension.

MINIFRAC TESTING

Minifrac testing was developed as a pretreatment technique for gaining information on fracture growth behavior.[48] This information is to be used in designing a fracturing treatment. Since its inception, various expansions, modifications, and refinements have increased its applications.[22,49-57] Papers have been published describing the application of minifrac analysis and its usefulness in determining fracture growth behavior.[58-60] By using these techniques to analyze the pressure decline during the shut-in period following the creation of a small test fracture or a full-scale fracture, parameters such as fracture width and length, fluid efficiency, and closure time may be determined. Of the parameters that may be inferred from minifrac analysis, the most useful, at least for design purposes, has been the effective fluid-loss coefficient.

Minifrac Procedures

Minifrac testing refers to three procedures that are mainly used to estimate the fracture extension pressure, effective fluid loss coefficients, and fracture closure pressure. These tests are step-rate, pump-in/flowback, and pump-in/shut-in.

1. Step-Rate Procedure

   This procedure is performed to estimate the fracture extension (fracture propagation) pressure and rate. An appropriate fluid is injected at low matrix flow rate (0.3 - 0.5 bbl/min). The injection rate is increased in increments (0.3 to 1.0 bbl/min), and the pressure is monitored throughout the procedure. The maximum pressure at each flow rate is plotted vs. the corresponding rate. Two lines usually fit the data; the intersection of these two lines yields the fracture extension pressure and rate. Figure 30 gives the illustration of step-rate test analysis.

2. Pump-In/Flowback Procedure

   This procedure can be performed after the completion of the step-rate test. When performed by itself, the pump-in/flowback test is performed by injecting an appropriate fluid at a rate that will extend the fracture. Approximately 50 to 100 bbl of fluid are pumped before the well is shut-in and the instantaneous shut-in pressure (ISIP) is recorded. The well is then flowed back at a constant rate (0.25 to 2.0 bbl/min) and the pressure is monitored. The fracture closure pressure is estimated from the plot of shut-in pressure vs. time as performed in the flowback case in microfrac tests. Figure 31 gives the illustration of closure-pressure determination from pump-in/flowback pressure decline.

3. Pump-in/shut-in Test

   Minifrac is often referred to as this procedure. Many researchers have devoted their time investigating pump-in/shut-in testing. We will devote the rest of the discussion for this section to this test.

Minifrac Analysis

Minifrac tests may be described as a test which incorporates two periods. In the first period, the formation under consideration is fractured and the fracture is extended. The well is then shut-in, and the pressure decline with time is observed and then analyzed.

To apply conventional minifrac analysis, the following basic assumptions are usually made.

1. The fracture has essentially constant height (or it radially propagates in case of penny-shaped fracture).
2. The fracture propagates through a semielastic media.
3. Injection rate is constant, and the injection fluid obeys the power-law model.
4. At shut-in, fracture stops propagation.
5. Injected fluid does not contain any appreciable amount of proppant. Thus, there is no proppant interference at closure.

Nolte described the original development of minifrac analysis using the Perkins and Kern[61] model. He developed type curves for analysis of the pressure decline. Nolte and other authors have expanded the original minifrac analysis to Kristianovitch and Zheltov models,[22,51] radial models,[22,51] and ellipsoidal models.[52,57] Although the type curves for various models are virtually identical, the equations used in the analysis are model dependent.

In the conventional approach of minifrac analysis, closure time may be calculated. However, unless the fluid leak-off is very slow the calculated volume will often be significantly longer than actual observed closure time. An alternate approach is to use observed closure time in performing the minifrac analysis instead of matching observed data against the theoretically developed type curves. The concept of using the observed closure time in analysis is based on the simple volume balance equation:

Injected Fluid = Leakoff during pumping + Leakoff during shut-in time at closure time

The use of observed closure time in that fashion implies that observed pressure decline matches reasonably well with the conventional type curve. This assumption is, sometimes, unrecognized by analysts. Thus, it is recommended that the analyst, at least qualitatively, perform type curve matching before using the closure time concept. Field practice has shown the observed closure pressure method to be superior for most higher leak-off reservoir conditions.

Major Modification to Minifrac Analysis

Close examination of minifrac analysis would reveal that it is implicitly assumed that the fracturing fluid is incompressible and the process is isothermal. These two assumptions may be violated in many instances, especially when using foam in the fracturing of fairly hot formations. Soliman[55] developed a technique to incorporate the effect of compressibility and temperature change into the equations describing pressure decline with time. The technique was successfully applied by Juranek *et al.*[59] in analyzing foam minfracturing tests.

It has been noticed that minifrac tests in naturally fractured formations usually may not be analyzed or may yield values that prove to be unrepresentative of the formation when attempting full-scale fractures. Shelly and McGowen[62] solved this problem by developing an empirical correlation describing specific formations. This technique has been applied in a variety of naturally fractured formations and has proven to be successful. The measure of success here means that the empirical correlation made it possible to successfully design a fracturing treatment that progressed as planned.

Soliman *et al.*[56] approached the problem in a different way. They assumed that leakoff rate into the formation is not necessarily inversely proportional to time. They hypothesized that the following equation should be used to describe leakoff rate as a function of time.

$$q \; \alpha \; \frac{C_{eff}}{t^{n}}$$

The leakoff exponent n is function of the formation and fracturing fluid. Soliman *et al.* presented the type curves for analysis of a minifrac test. Their solution may be considered a general solution, while the conventional solution is a special solution for n = 0.5.

Optimum Fracture Treatment Design Utilizing Minifrac Analysis

Fluid loss plays an important role in the design of hydraulic fracturing treatment. If the fluid loss is large in a given formation, the fracturing design should be such that it compensates for high fluid loss. This can be achieved by considering the following factors:

1. Increasing the injection rate.

2. Increasing the pre-pad and/or the pad volume and, in general, increasing the total volume.

3. Increasing viscosity and/or adding fluid-loss additives.

Minifrac testing can help identify a feasible fracturing fluid and/or show if fluid loss additives are needed. The minifrac test is completed and pressure fall-off is observed. Sharp pressure fall-off signals high fluid loss and warrants addition of an increase in fluid loss additive concentration. From the pressure fall-off analysis the fracture closure pressure (FCP) is determined using pressure vs. square root of time method. Ideally, the actual fracture height is measured using temperature or radioactive logs. Reservoir data, minifrac treatment data, actual fracture height, net fluid loss height, and fracture closure pressure are entered into the minifrac simulator based on theories developed by either Nolte[22] or Lee.[51-53] Fluid leak-off coefficient and fluid efficiency are the main output of the simulator.

The optimum fracture design is attained by following the steps given below:

1. Use radial flow and fracture well reservoir simulators to select an economically desirable fracture length and conductivity.

2. Use the following equation to calculate the percent pad volume using the minifrac fluid efficiency.

$$V_p = \left[1 - \left(\frac{E_f}{100} \right) \right]^2 + 0.05$$

where:

E_f	=	Fluid efficiency
V_p	=	Percent pad volume

3. Pick a reasonable fracturing treatment with a pad volume and proppant schedule using information gained in 2.

4. Pertinent information obtained from minifrac test and fracturing treatment schedule chosen in Step 3 are used in a fracture design simulator to determine pumping schedule needed to achieve the desired fracture length and conductivity.

5. Repeat Steps 3 and 4 until length and fracture conductivity in 1 and 4 match reasonably well.

CONCLUSIONS

In this paper, we discussed the subjects of microfrac testing, anelastic strain recovery, full-wave sonic log, and minifrac testing. The following information was covered.

1. Summarized practical engineering methods to determine in-situ stresses, magnitude, and, in some instances, direction.

2. Applications of these methods to assist in hydraulic fracturing treatment design were presented.

3. Recommended procedures to analyze data needed for fracture design are given. These procedures have been acquired through practical experience in the area of hydraulic fracturing.

REFERENCES

1. Gidley, J.L., Holditch, S.A., Nierode, D.E., and Veatch Jr., R.W.: "*Recent Advances in Hydraulic Fracturing*," Monograph Series, SPE, Richardson, TX (1989) **12**.

2. Lemon, R.F., Patel, H.J., and Dempsey, J.R.: "Effects of Fracture and Reservoir Parameters on Recovery From Low Permeability," paper SPE 5111 presented at the 1974 SPE Annual Meeting, Houston, Oct. 6-9.

3. Holditch, S.A.: *Quarterly Low-Permeability Gas Well Research Report* (Fall 1975), quarterly report, Petroleum Engineering Department, Texas A&M University, College Station.

4. "The Fracbook™ Design/Data Manual for Hydraulic Fracturing," Halliburton Services, Duncan (1971).

5. Rice, J.R.: "*Mathematical Analysis in the Mechanics of Fracture*," Tretise on Fracture, Academic Press, Inc., New York (1962) **2**, Ch. 3, 191.

6. Simonson, E.R.: "Containment of Massive Hydraulic Fractures," *SPEJ* (Feb. 1978) 27-32.

7. Ahmed, U., Newberry, B.M., and Cannon D.E.: "Hydraulic Fracture Treatment Design of Wells with Multiple Zones," paper SPE/DOE 13857 presented at the 1985 Low Permeability Gas Reservoirs Meeting, Denver, May 19-22.

8. Hubert, M.K. and Willis, D.G.: "Mechanics of Hydraulic Fracturing," *Trans.*, AIME (1957) **210**, 153-66.

9. Fairhurst, C.: "Measurement of In-Situ Rock Stresses, with Particular Reference to Hydraulic Fracturing," *Rock Mechanics and Engineering Geology* (1964) **2**, 129-47.

10. Kehle, R.O.: "Determination of Tectonic Stresses Through Analysis of Hydraulic Well Fracturing," *Journal of Geophysical Research* (1964) **69**, 259-73.

11. Kuhlman, R.D.: "Microfrac Tests Optimize Frac Jobs," *Oil & Gas J.* (Jan. 22, 1990) 45-49.

12. Daneshy, A.A., Chisholm, P.T., Slusher, G.L., and Magee, D.A.: "In-Situ Stress Measurements During Drilling," *JPT* (Aug. 1986) 891-898.

13. McLennan, J.D. and Roegiers, J.C.: "How Instantaneous are Instantaneous Shut-In Pressures?," paper SPE 11064 presented at the 1982 SPE Annual Technical Conference and Exhibition, New Orleans, Sept. 26-29.

14. Gronseth, J.M. and Kry, P.R.: "Instantaneous Shut-In Pressure and its Relationship to the Minimum In-Situ Stress," *Proc. Workshop on Hydraulic Fracture Stress Measurements*, Open-File Rept. 82-1075 (1982), 147-67, U.S. Geological Survey, Washington, DC.

15. McLennan, J.D.: "A Fracture Mechanics Approach," PhD thesis, University of Toronto, Toronto (1980).

16. Zoback, M.D. and Haimson, B.C.: "Status of the Hydraulic Fracturing Method for In-Situ Stress Measurements," *Proc.*, 23rd U.S. Symposium on Rock Mechanics (1982), University of California, Berkeley, 143-56.

17. Doe T.W.: "Determination of the State of Stress at the Stripa Mine, Sweden," *Proc. Workshop on Hydraulic Fracturing Stress Measurements*, Open-File Rept 82-1075 (1982), 394-403, U.S. Geological Survey, Washington, DC.

18. McLennan, J.D. and Roegiers, J.C.: "Do Instantaneous Shut-In Pressures Accurately Represent the Minimum Principal Stress," *Proc. Workshop on Hydraulic Fracturing Stress Measurements*, Open-File Rept 82-1075 (1982), 181-208, U.S. Geological Survey, Washington, DC.

19. Aamondt A. and Kuriyagawa, M.: "Measurement of Instantaneous Shut-In Pressure in Crystalline Rock," *Proc. Workshop on Hydraulic Fracturing Stress Measurements*, Open-File Rept 82-1075 (1982), 394-403, U.S. Geological Survey, Washington, DC.

20. Aggson, J.R. and Kim, K.: "Analysis of Hydraulic Fracturing Pressure Histories: A Comparison of Five Methods Used to Identify Shut-In Pressure," *Int. J. Rock Mech. Min. Sci. and Geomech. Abstr.* (1987), Vol. 24, 75-80.

21. Cinco-Ley, H., Samaniego-V., F., and Dominguez, N.: "Transient Pressure Behavior for a Well with a Finite Conductivity Vertical Fracture," *SPEJ* (Aug. 1978) 253-64.

22. Nolte, K.G.: "A General Analysis of Fracturing Pressure Decline with Application to Three Models," *SPE Formation Evaluation* (Dec. 1986) **1**, 571-83.

23. Jones, C. and Sargeant, J.P.: "Obtaining The Minimum Horizontal Stress From Microfrac Test Data: A New Approach Utilizing a Derivative Algorithm," paper SPE 18867 presented at the 1989 SPE Production Operations Symposium, Oklahoma City, March 13-14.

24. Warpinski, N.R., Branagan, P., and Wilmer, R.: "In-Situ Stress Measurements at DOE's Multiwell Experiment Site, Mesaverde Group, Rifle, Colorado," paper SPE 12142 presented at the 1983 SPE Annual Technical Conference and Exhibition, San Francisco, Oct. 5-8.

25. Whitehead, W.S., Hunt, E.R., and Holditch, S.A.: "The Effects of Lithology and Reservoir Pressure on the In-Situ Stresses in the Waskom (Travis Peak) Field," paper SPE/DOE 16403 presented at the 1987 Low Permeability Reservoir Symposium, Denver, May 18-19.

26. Shlyapaborsky, J., Walhaug, W.W., Sheffield, R.E., and Huckabee, P.T.: "Field Determination of Fracturing Parameters for Overpressure Calibrated Design of Hydraulic Fracturing," paper SPE 18195 presented at the 1988 SPE Annual Technical Conference and Exhibition, Houston, Oct. 2-5.

27. Obert, L. and Duvall, W.I.: *Rock Mechanics and the Design of Structures in Rock*, John Wiley and Sons, New York (1967) 409-459.

28. Teufel, L.W.: "Determination of In-Situ Stress From Anelastic Strain Recovery Measurements of Oriented Core," paper SPE 11649, presented at the 1983 SPE/DOE Symposium on Low Permeability Gas Reservoirs, Denver, March 14-16.

29. Teufel, L.W.: "In-Situ Stress State in the Mounds Test Well as Determined by the Anelastic Strain Recovery Method," paper SPE 13896 presented at the 1985 SPE/DOE Symposium on Low Permeability Gas Reservoirs, Denver, May 19-22.

30. El Rabaa, A.W.M. and Meadows, D.L.: "Laboratory and Field Applications of the Strain Relaxation Method," paper SPE 15072 presented at the 1986 SPE Annual Technical Conference and Exhibition, Oakland, CA, April 2-4.

31. Blanton, T.L.: "The Relation Between Recovery Deformation and In-Situ Stress Magnitudes," paper SPE/DOE 11624 presented at the 1983 Symposium on Low Permeability, Denver, March 14-16.

32. El Rabaa, W.: "Determination of the Stress Field and Fracture Direction in the Danian Chalk," *ISRM - SPE*, 1989 International Symposium on Rock at Greate Depth, **2**, 1017-24, Pau, France Aug 28-31.

33. Ramos, G.G. and Rathmell, J.J.: "Effects of Mechanical Anisotropy on Core Strain Measurements for In-Situ Stress Determination," paper SPE 19593 presented at the 1989 SPE Annual Technical Conference and Exhibition, San Antonio, TX, Oct. 8-11.

34. Montmayeur, H. and Graves, R.M.: "Prediction of Static Elastic / Mechanical Properties of Consolidated and Unconsolidated Sands, Acoustic Measurements: Correlations," paper SPE 15644 presented at the 1986 SPE Annual Technical Conference and Exhibition, New Orleans, Oct. 5-6.

35. van Heerdan, W.J.: "General Relationships Between Static and Dynamic Moduli of Rock," *Int. Jour. Rock Mech. Min. Sci. & Geomech.* (1987) 24, No. 6, 381-85.

36. Labudovie, V.: "The Effect of Poisson's Ratio on Fracture Height," *JPT*, (Feb. 1984) 287-90.

37. Minear, J.W.: "Technical Memorandum on Poisson's Ratio," Internal Publication, Halliburton Logging Services (Jan. 1981).

38. Johnston, D.H.: "Physical Properties of Shale at Temperature and Pressure," *Geophysics* (1987) **52**, No. 10, 1391-1401.

39. Gregory, A.R.: "Fluid Saturation Effects on Dynamic Elastic Properties of Sedimentary Rocks," *Geophysics* (Oct. 1976) **41**, No. 5, 895 - 921.

40. Terzaghi, K.: *Theoretical Soil Mechanics*, John Wiley and Sons Inc., New York (1943).

41. Handin, J., Hager, R.V. Jr., Friedman, M., and Feather, J.N.: "Experimental Deformation of Sedimentary Rocks Under Confining Pressure: Tests at High Temperature," *Bulletin American Association of Petroleum Geology* (1963) **42**, No. 12, 2892-2934.

42. Roegiers, J.C.: "Elements of Rock Mechanics," *Reservoir Stimulation*; Sch. Ed. Services, Houston (1987) 2-1 - 2-21.

43. Toksoz, M.N. and Cheng, C.H.: "Modeling of Seismic Velocities in Porous Rocks and its Application to Seismic Exploration," *The Arabian Journal for Science and Engineering Special Issue* (1978), 109-31.

44. Anderson, R.A.: "Fluid And Frequency Effects On Sonic Velocities," paper AAA presented at the 1984 SPWLA 25th Annual Logging Symposium, New Orleans, June 10-13.

45. Prats, M.: "Effect of Burial History on the Subsurface Horizontal Stresses of Formations Having Different Material Properties," *SPEJ* (Dec. 1981) 658-62.

46. Ahmed, U., Markley, M.E., Crary, S.F. and Liu, O.Y.: "Enhanced In-Situ Stress Profiling Using Microfrac, Core, and Sonic Logging Data," paper SPE 19004 presented at the 1989 SPE Rocky Mountain Low Permeability Reservoir Symposium, Denver, March 6-8.

47. McLellan, P.: "In-situ Stress Prediction and Measurement by Hydraulic Fracturing, Wapiti, Alberta," *Jour. Can. Pet. Tech.*, (Mar.-Apr. 1988) 27, No. 2, 85-95.

48. Nolte, K.G.: "Determination of Fracture Parameters From Fracturing Pressure Decline," paper SPE 8341 presented at the 1979 SPE Annual Technical Conference and Exhibition, Las Vegas, Sept. 23-26.

49. Nolte, K.G.: "Application of Fracture Design Based on Pressure Analysis," *SPEPE* (Feb. 1988) 31-42; *Trans.*, AIME, **285**.

50. Nolte, K.G.: "Determination of Proppant and Fluid Schedules From Fracturing-Pressure Decline," *SPEPE* (July 1986) 255-65; *Trans.*, AIME, **283**.

51. Lee, W.S.: "Pressure Decline Analysis with the Khristianovich and Zheltov and Penny-Shaped Geometry Model of Fracturing," paper SPE 13872 presented at the 1985 SPE/DOE Symposium on Low Permeability Gas Reservoirs, Denver, May 19-22.

52. Lee, W.S.: "Minifracture Analysis Based on Ellipsoidal Geometry," paper SPE 15369 presented at the 1986 SPE Annual Technical Conference and Exhibition, New Orleans, Oct. 5-8.

53. Lee, W.S.: "New Method of Minifracture Analysis Offers Greater Accuracy and Enhanced Applicability," paper SPE 15941 presented at the 1986 SPE Eastern Regional Meeting, Columbus, OH, Nov. 12-14.

54. Lee, W.S.: "Study of the Effects of Fluid Rheology on Minifracture Analysis," paper SPE 16916 presented at the 1987 SPE Annual Technical Conference and Exhibition, Dallas, Sept. 27-30.

55. Soliman, M.Y.: "Technique for Considering Fluid Compressibility and Temperature Changes in Minifracture Analysis," paper SPE 15370 presented at the 1986 SPE Annual Technical Conference and Exhibition, New Orleans, Oct. 5-8.

56. Soliman, M.Y., Poulsen, D.K., and Kuhlman, R.D.: "General Minifrac Analysis for Heterogeneous Formation Including Spurt Loss," paper SPE 20705 presented at the 1990 SPE Annual Technical Conference and Exhibition, New Orleans, Sept. 23-26.

57. Martins, J.P. and Harper, T.R.: "Mini-Frac Pressure Decline Analysis for Fractures Evolving From Long Perforated Intervals and Unaffected by Confining Strata," paper SPE 13869 presented at the 1985 SPE/DOE Symposium on Low Permeability Gas Reservoirs, Denver, May 19-22.

58. Tan, H.C., McGowen, J.M., and Soliman, M.Y.: "Field Application of Minifracture Analysis to Improve Fracturing Treatment Design," *SPEPE* (May 1990) 125-32.

59. Juranek, T.A., Llewellyn, M.T., Drescher, G.P., Tan, H.C., and McGowen, J.M.: "Minifracture Analyses and Stimulation Treatment Results for CO_2 - Energized Fracturing Fluids in South Texas Gas Reservoirs," paper SPE 20706 presented at the 1990 SPE Annual Technical Conference and Exhibition, New Orleans, Sept. 23-26.

60. Nolte, K.G.: "Fracture Design Considerations Based on Pressure Analysis," paper SPE 10911 presented at the 1982 SPE Cotton Valley Symposium, Tyler, TX, May 20.

61. Perkins, T.K. and Kern, L.R.: "Widths of Hydraulic Fractures," *JPT* (Sept. 1961) 937-49; *Trans.*, AIME, 222.

62. Shelley, R.F. and McGowen, J.M.: "Pump-In Test Correlation Predicts Proppant Placement," paper SPE 15151 presented at the 1986 SPE Rocky Mountain Regional Meeting, Billings, MT, May 19-21.

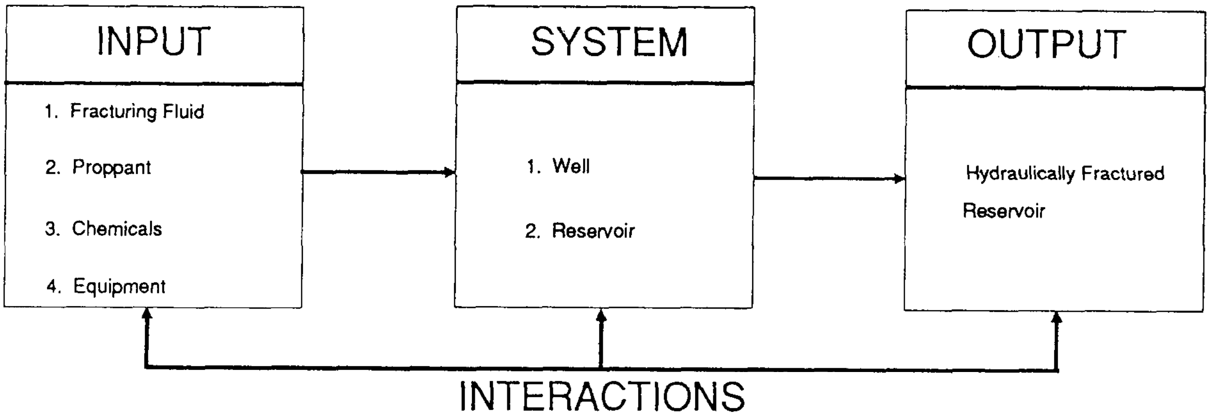

Figure 1 - Hydraulic fracturing process

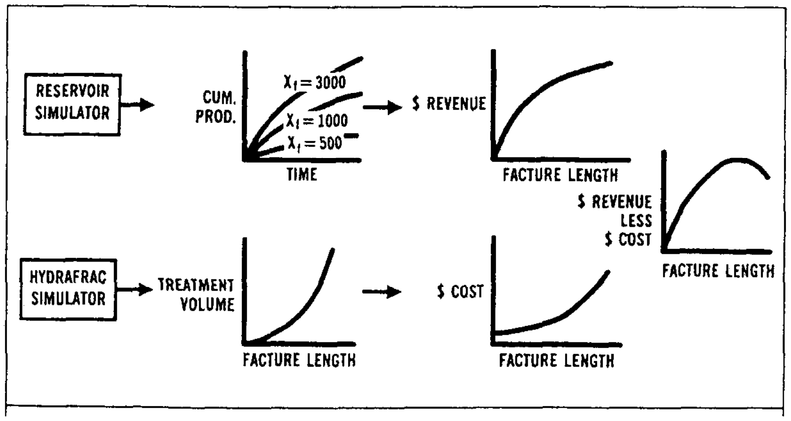

Figure 2 - Production optimization[1]

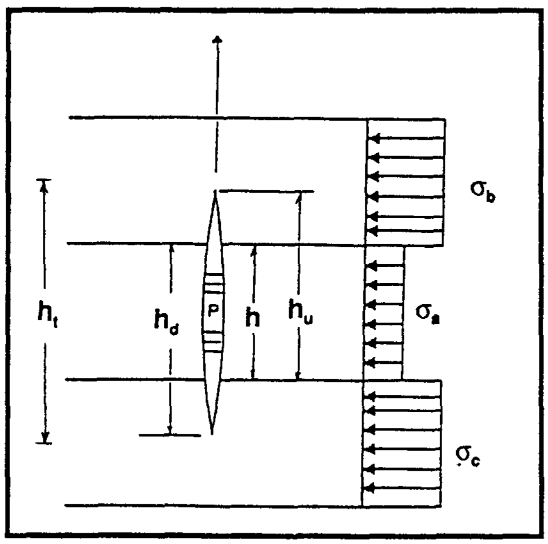

Figure 3 - Fracture height

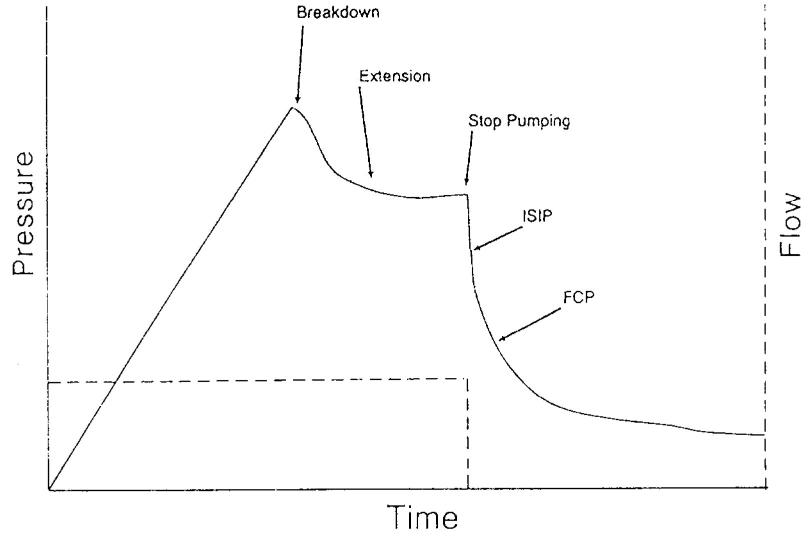

Figure 4 - Microfrac pressure behavior

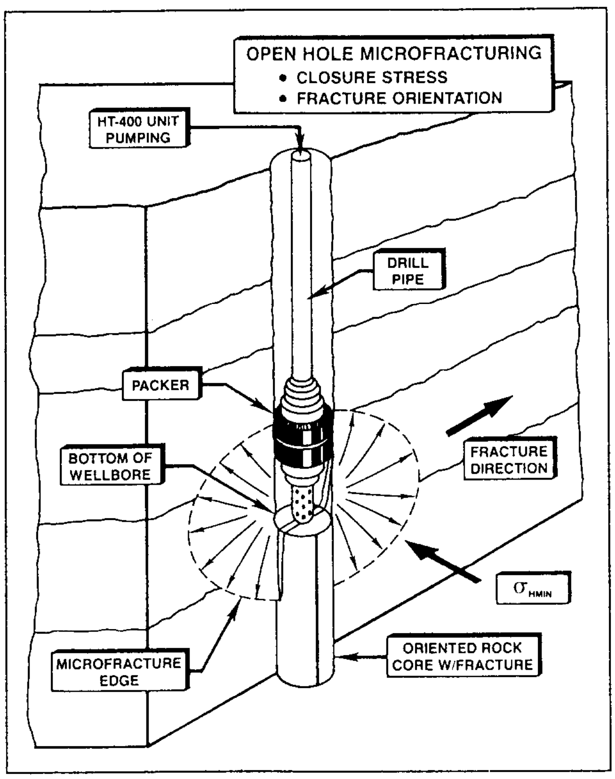

Figure 6 - Open hole microfracturing[11]

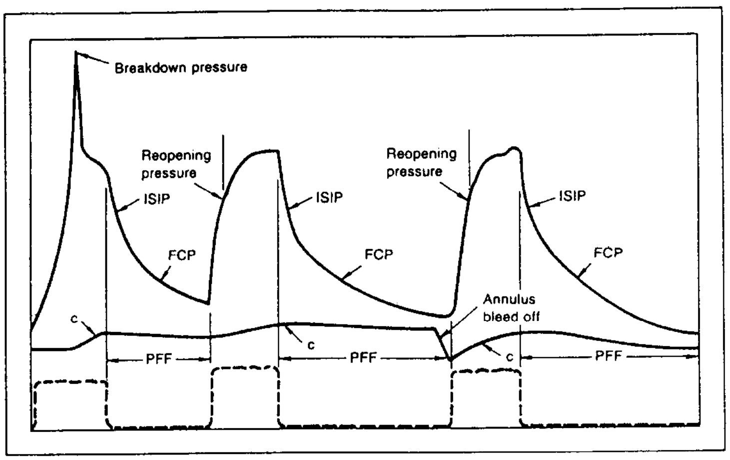

Figure 5 - Pressure response in microfracturing process

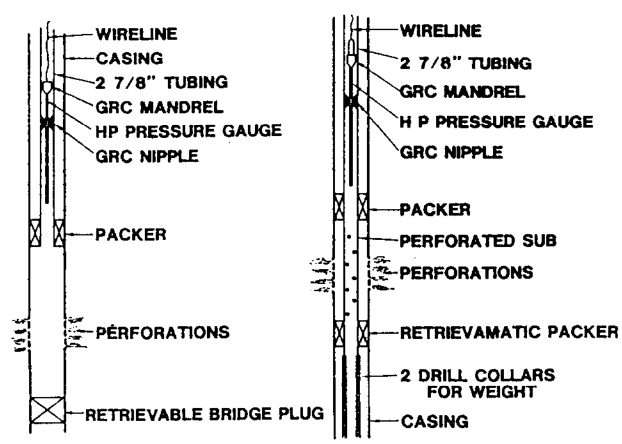

a) PACKER AND BRIDGE PLUG

b) STRADDLE PACKERS

Figure 7 - Downhole equipment for cased-hole microfracturing[24]

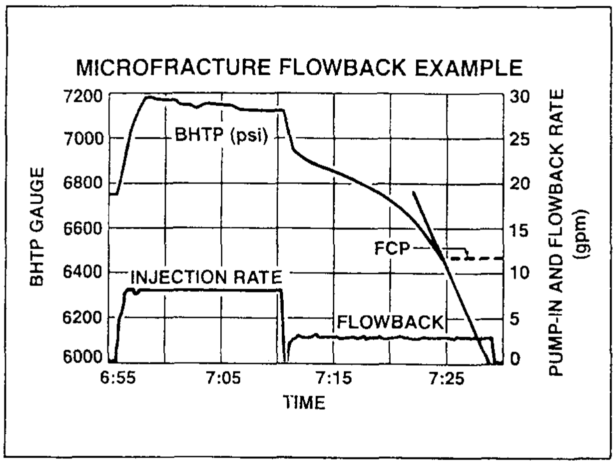

Figure 8 - Microfrac flowback pressure profile[10]

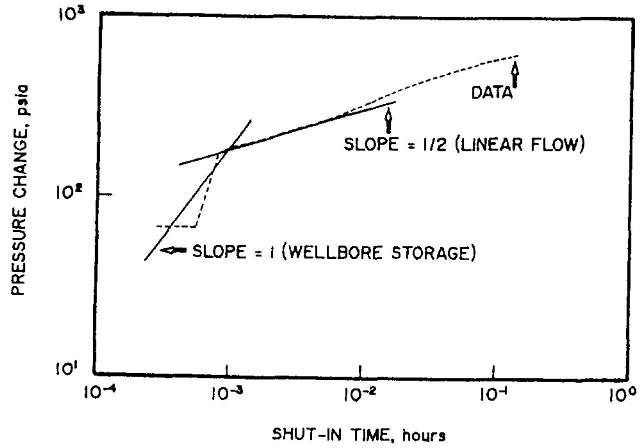

Figure 9 - Flow regime change - log-log plot of fall-off pressure[25]

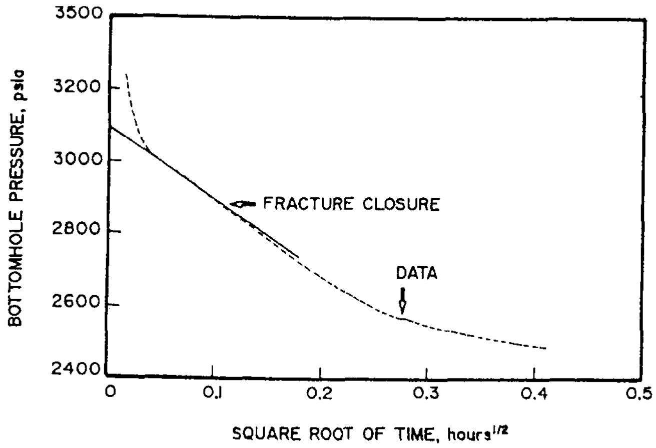

Figure 10 - Flow regime change - square root of time[25]

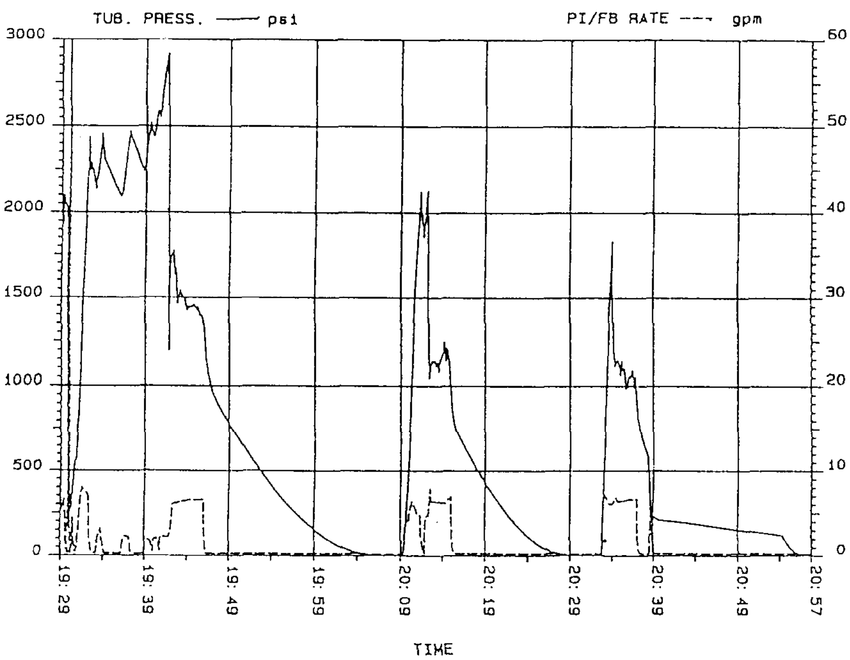

Figure 11 - Pressure and rate vs. time for 3 microfrac stages

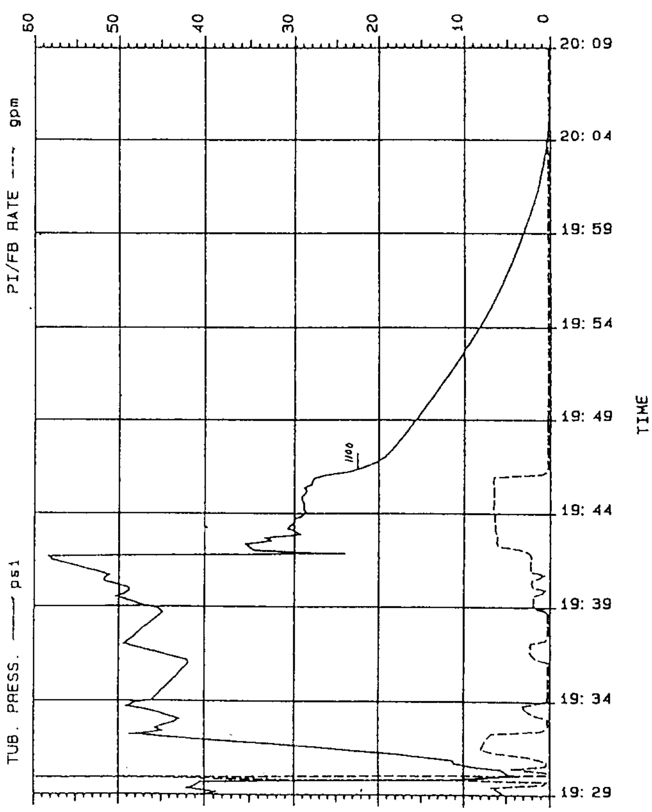

Figure 12 - Pressure and rate vs. time for stage 1

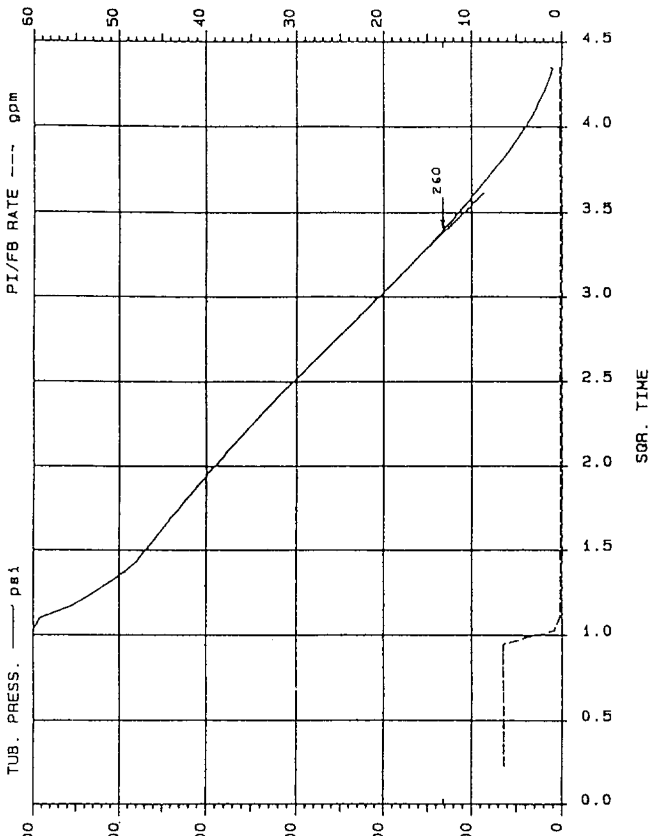

Figure 13 - Pressure vs. $\sqrt{\text{time}}$ for stage 1

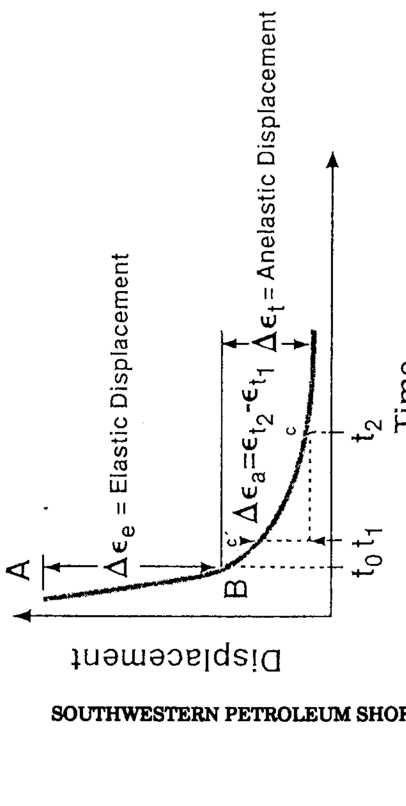

Figure 14 - Elastic and anelastic displacements

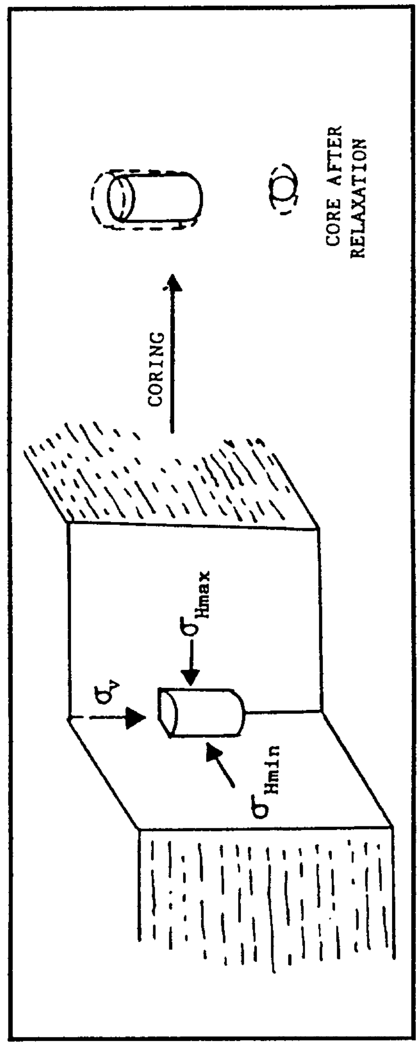

Figure 15 - Core relaxation

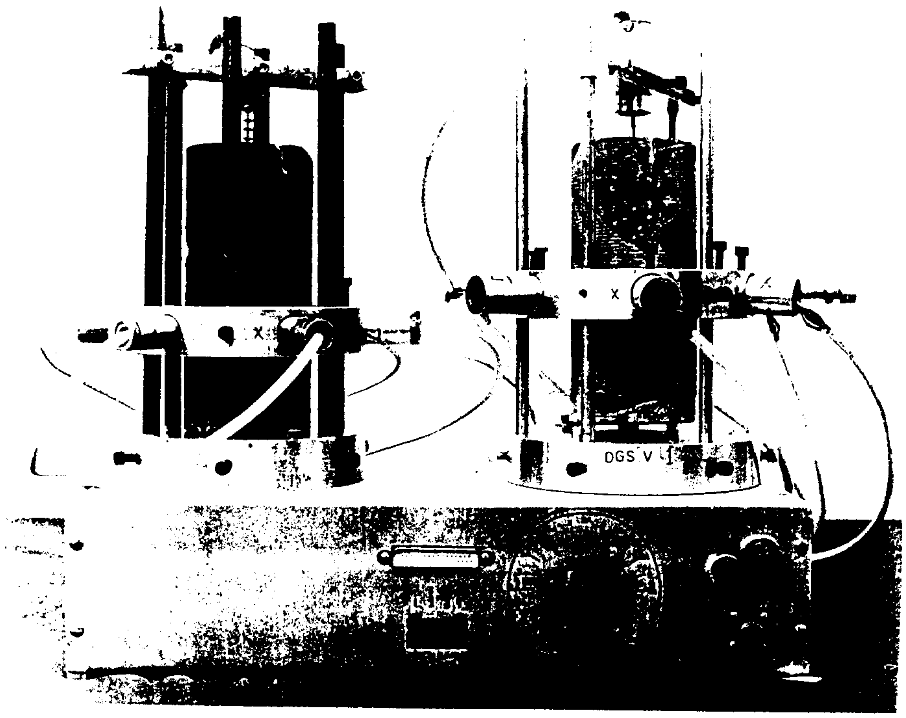

Figure 16 - Vertical hole sample apparatus

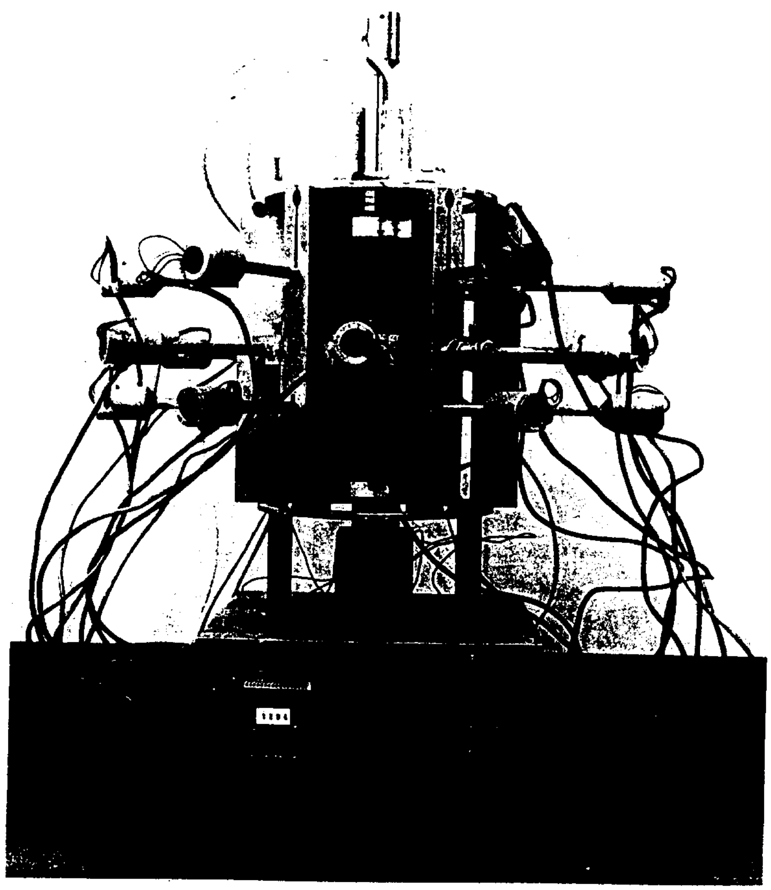

Figure 17 - Deviated hole sample apparatus

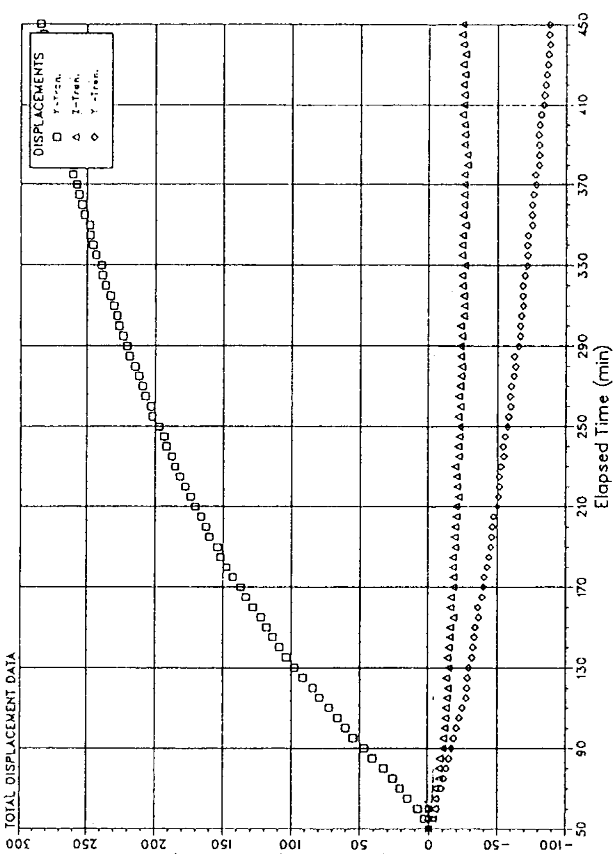

Figure 18 - Voltage corrected displacements

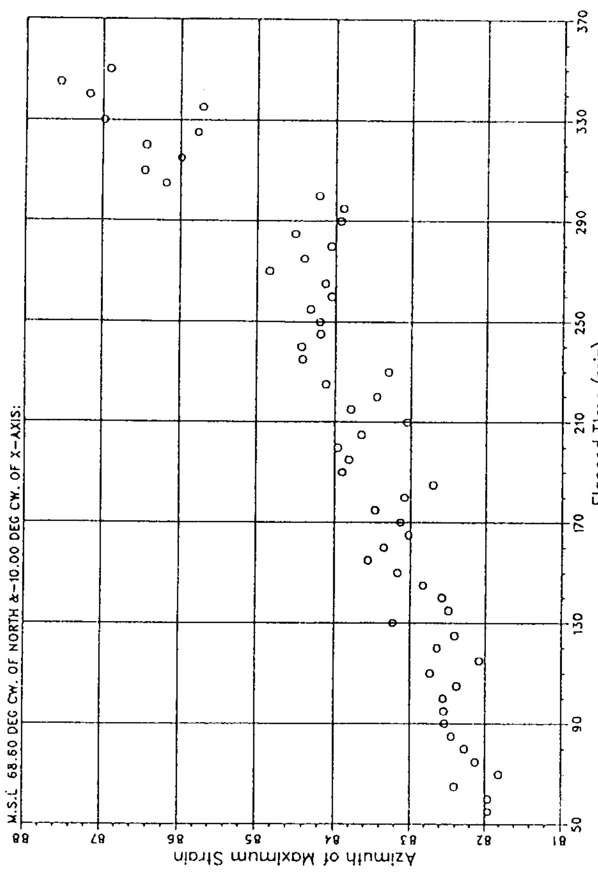

Figure 19 - Maximum strain angles based on "differential" (STEP = 20)

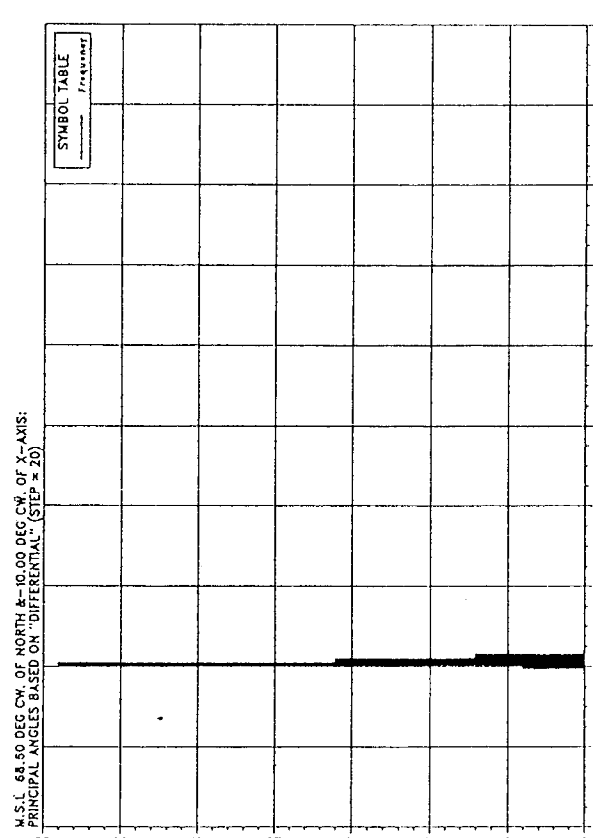

Figure 20 - Maximum strain azimuth vs. frequency

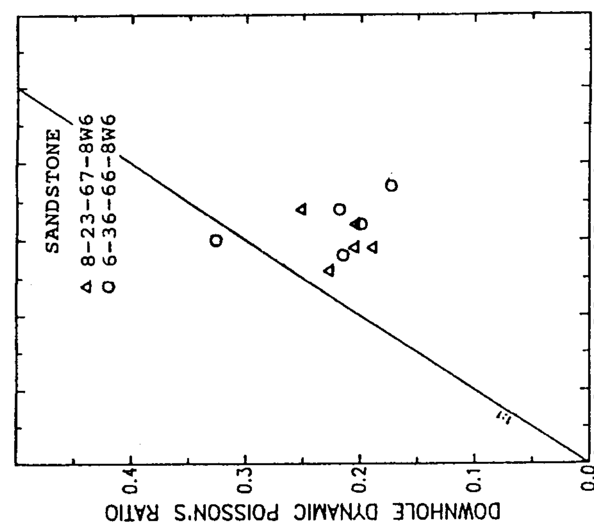

Figure 21 - Crossplot of static Poisson's ratio and dynamic Poisson's ratio (sonic log), Cardium sandstone - core plugs were orientated vertically.[7]

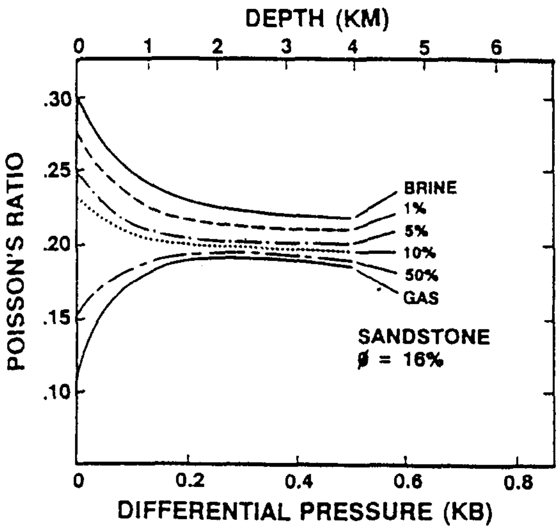

Figure 22 - The gas effect on Poisson's ratio decreases with increasing depth. Model of a 16% porosity sandstone[43]

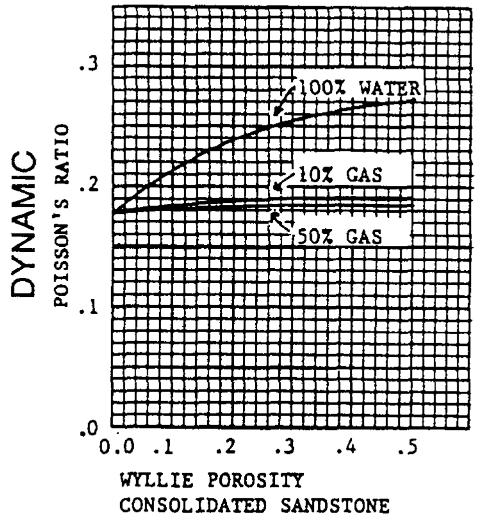

Figure 23 - The gas effect on Poisson's ratio declines with decreasing porosity[44]

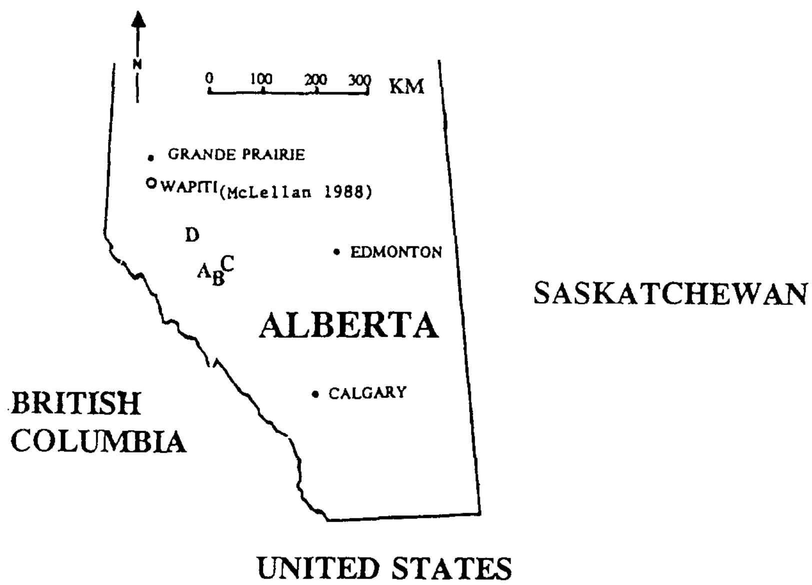

Figure 24 - Location of case example wells (A, B, C and D) and McLellan's[47] Cardium well at Wapiti. The data from these wells are plotted in Figures 25 and 26.

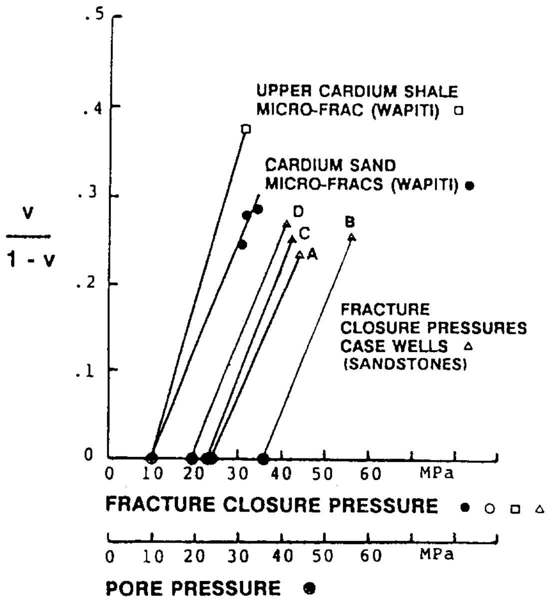

Figure 25 - Plot of FCP and p vs. $\frac{V}{1-V}$

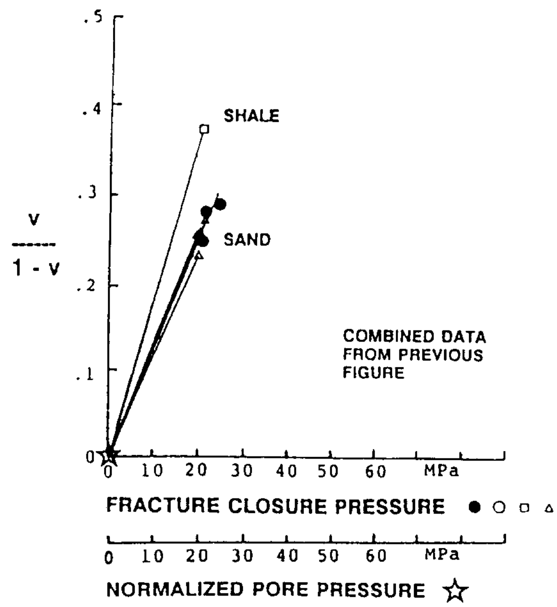

Figure 26 - FCP vs. $\frac{V}{1-V}$ plot

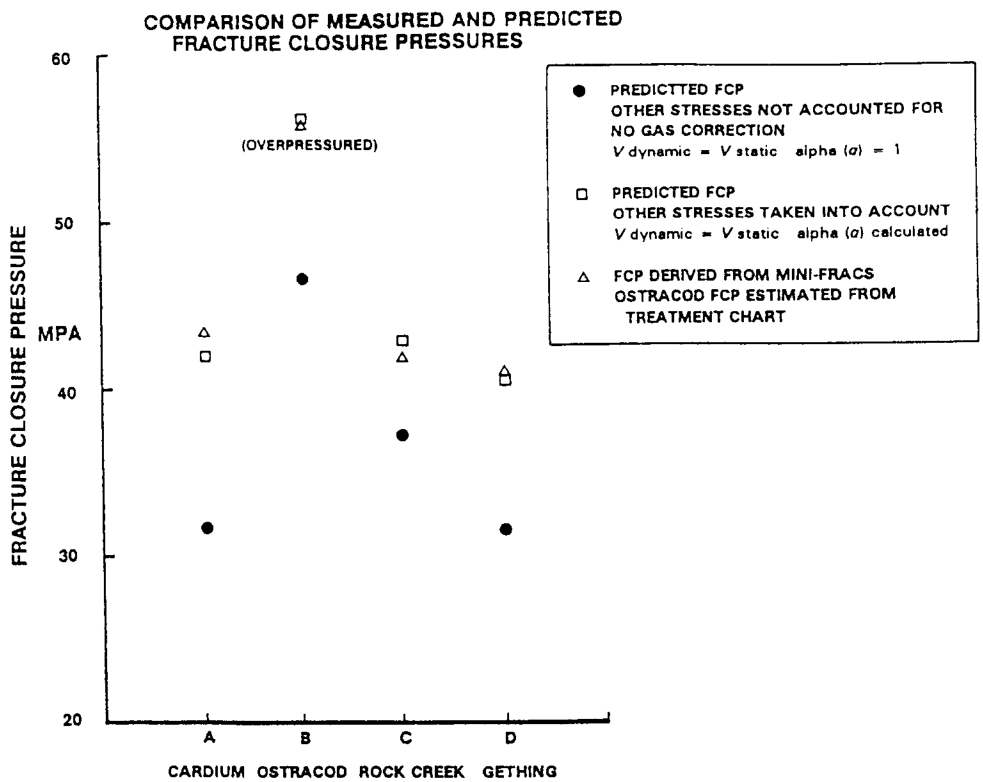

Figure 27 - (Case examples A, B, C, & D) Predicted fracture closure pressures, both corrected and uncorrected for other stresses, are summarized here. Corrected fracture closure pressures derived from minifrac data.

Tool Specifications

Outside Diameter	3⅝ in	92 mm
Approximate Overall Length*		
Standard Configuration	564 in	14.33 m
Extra-Long Cased Hole Configuration	654 in	16.61 m
Temperature Rating	400°F	204°C
Pressure Rating	20,000 psi	137,900 kPa 1,406 kg/cm2
Recommended Logging Speed	30 ft/min	9.1 m/min
Recommended Hole Sizes		
Minimum Borehole Diameter	5.875 in	149 mm
Maximum Borehole Diameter	20 in	508 mm
Centering	Centered	
Transmitter		
Type	Piezoelectric, metal-covered	
Resonant Frequency	13 kHz	
Receivers		
Type	Piezoelectric, metal-covered	
Frequency Response	Flat from 700 Hz to 30 kHz	
Transmitter-to-Receiver Offsets		
Standard Configuration	10, 11, 12, and 13 ft (3.05, 3.35, 3.66, and 3.96 m)	
Extra-Long Cased Hole Configuration	17.5, 18.5, 19.5, and 20.5 ft (5.33, 5.64, 5.94, and 6.25 m)	

Length includes gamma ray and Digital Interactive Telemetry System unit.

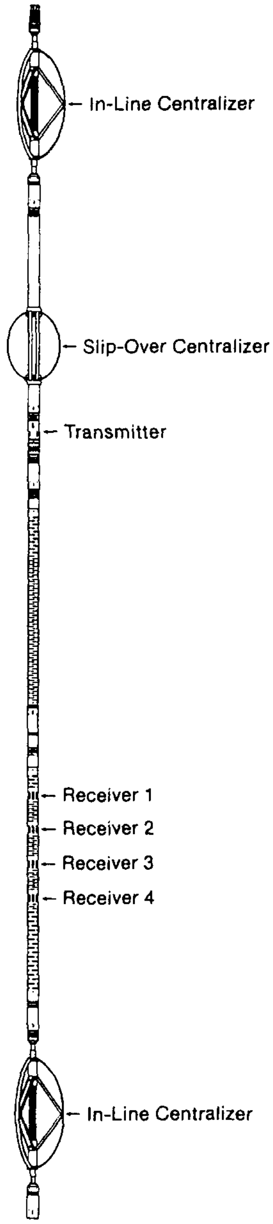

Figure 28 - A typical full-wave logging tool (Halliburton Logging Services)

McLELLAN'S WAPITI WELL

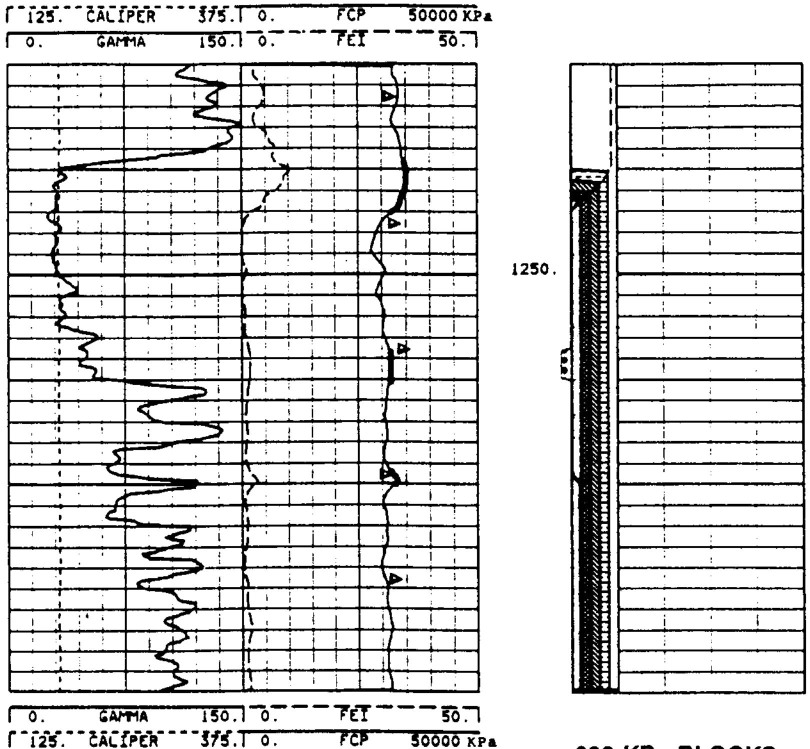

MICRO-FRAC DATA △

Figure 29 - Field example[47]

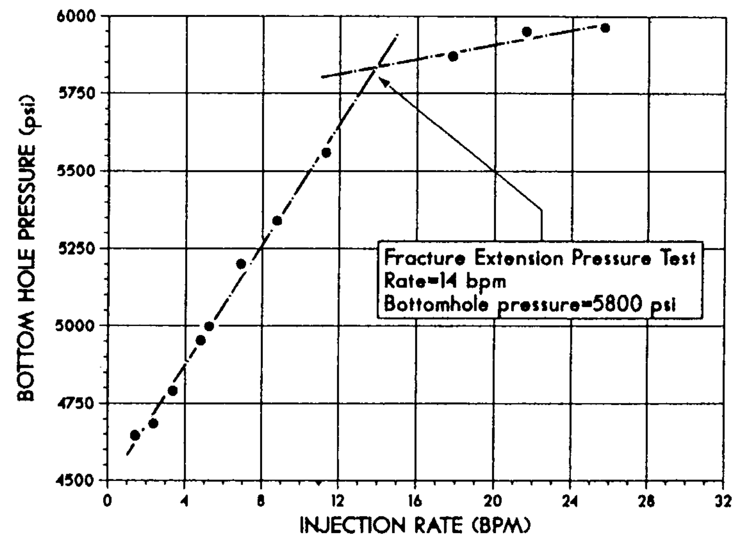

Figure 30 - Illustration of step-rate test analysis[58]

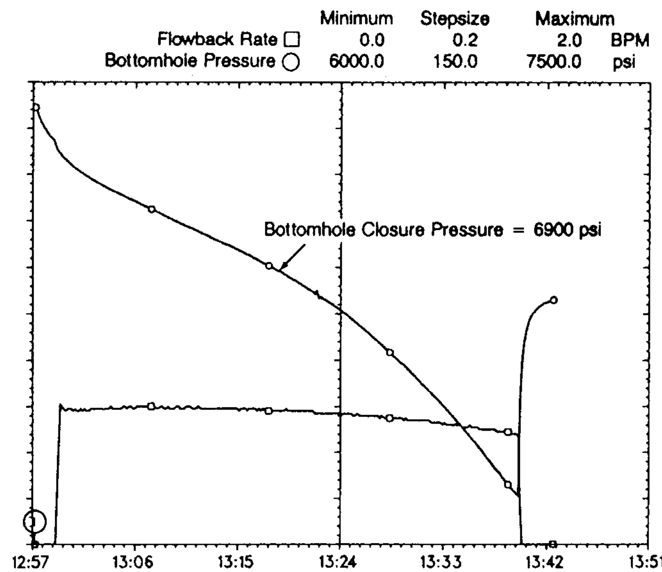

Figure 31 - Closure=pressure determination from pump-in-flowback pressure decline[58]